

increases from single-layer to four or more-layer cloud occurrence. Further, the vertical structure of clouds is also studied with respect to the arrival date of Indian summer monsoon over Gadanki.

Keywords: Cloud vertical structure, Single-layer clouds, Multi-layer clouds, Cloud base, top and thickness

1. Introduction

Clouds are vital in driving the climate system as they play important role in radiation budget, general circulation and hydrological cycle (Ramanathan et al., 1989; Rossow and Lacis, 1990; Wielicki et al., 1995; Li et al., 1995; Stephens, 2005; Yangetal., 2010; Huang,2013). By interacting with both shortwave and long-wave radiation, clouds play crucial role in the radiative budget at the surface, within and at the top of the atmosphere (Li et al., 2011; Ravi Kiran et al., 2015; George et al., 2018). Clouds result from the water vapor transports and cooling by atmospheric motions. The forcing for the atmospheric circulation is significantly modified by vertical and horizontal gradients in the radiative and latent heat fluxes induced by the clouds (Chahine et al., 2006 and Li et al., 2005). The complexity of the processes involved, the vast amount of information needed, including vertical and spatial distribution, and the uncertainty associated with the available data, all add difficulties to determine how clouds contribute to climate change (e.g., Heintzenberg and Charlson, 2009). In particular, knowledge about cloud type is very important, because the overall impact of clouds on the Earth's energy budget is difficult to estimate, as it involves two opposite effects depending on cloud type (Naud et al., 2003). Low, highly reflective clouds tend to cool the surface, whereas high, semi-transparent clouds tend to warm it, because they let much of the shortwave radiation through but are opaque to the longwave radiation. Whereas deep convective clouds (DCCs) neither warm nor cool the surface, because their cloud greenhouse

and albedo forcing's nearly balance. However, DCCs produce fast vertical transport, redistribute water vapor and chemical constituents, and influence the thermal structure of the Upper Troposphere and Lower Stratosphere (UTLS) (Biondi et al., 2012).

Changes in the cloud vertical structure (locations of cloud top and base, number and thickness of cloud layers) affect the atmospheric circulations by modifying the distribution of radiative and latent heating rates within the atmosphere (e.g., Slingo and Slingo, 1988; Randall et al., 1989; Slingo and Slingo, 1991; Wang and Rossow, 1998; Li et al., 2005 and Chahine et al., 2006; Cesana and Chepfer, 2012; Rossow and Zhang, 2010; Rossow et al., 2005; Wang et al., 2014b). The effects of cloud vertical structure (CVS) on atmospheric circulation have been described using atmospheric models (e.g., Rind and Rossow, 1984 and Crewell et al., 2004) ~~many authors~~. Crewell et al. (2004) underlined the importance of clouds in multiple scattering and absorption of sunlight, processes that have a significant impact on the diabatic heating in the atmosphere. The vertical gradients of diabatic heating in the cloud distribution were more important to the circulation strength than horizontal gradients (Rind and Rossow, 1984). These complex phenomena are not yet fully understood and are subject to large uncertainties. In fact, the assumed or computed vertical structure of cloud occurrence in general circulation models (GCMs) is one of the main reasons for the differences in modeled projections of future climate. For example, most GCMs underestimate the cloud cover, while only a few overestimate it (Xi et al., 2010). Therefore, to improve the understanding of cloud-related processes, and then to increase the predictive capabilities of large-scale models (including global circulation models), better and more accurate observations of CVS are needed. The present work reports the diurnal and seasonal variations in CVS over Gadanki using long-term high vertical resolution radiosondes observations.

Ground-based instruments (e.g. Warren et al., 1988; Hahn et al., 2001), active sensor satellites (e.g. Stephens et al., 2008; Winker et al., 2007) and upper air measurements from

76 radiosondes (Wang et al., 2000) are usually applied to observe the CVS. Ground-based
77 instruments such as lidar, cloud radar and ceilometers provide cloud measurements with
78 continuous temporal coverage. Lidars and ceilometers are very efficient in detecting clouds
79 and can locate the bottom of cloud layer precisely, but cannot usually detect the cloud top,
80 due to attenuation of the beam within the cloud. The vertically pointing cloud radar is able to
81 detect the cloud top, although signal artifacts can cause difficulties during precipitation
82 (Nowak et al., 2008). On the other hand, passive sensor satellite data, such as from ISCCP
83 (the International Satellite Cloud Climatology Project) and MODIS (the Moderate Resolution
84 Imaging Spectroradiometer), have some limitations in using the analyses presented in this study.
85 For example, the thin clouds are indistinguishable from aerosols in ISCCP when optical
86 thickness is less than 0.3–0.5) (Rossow and Garder, 1993); Both ISCCP and MODIS
87 underestimate low-level clouds and overestimate middle-level cloud (Li et al., 2006; Naud
88 and Chen, 2010). Hence, conventional passive-sensor satellite measurement, largely miss the
89 comprehensive information on the vertical distribution of cloud layers. The precipitation
90 radar and TRMM Microwave Imager on-board the Tropical Rainfall Measuring Mission
91 (TRMM) satellite are helpless in observing small-size particles despite of its capability of
92 penetrating rainy cloud and obtaining the internal three-dimensional information, and only
93 larger rainfall particles can be observed due to limitations of its working broadband. On the
94 other hand, active sensors such as the Cloud Profiling Radar (CPR) on CloudSat and the
95 Cloud-Aerosol Lidar with Orthogonal Polarization (CALIOP) aboard CALIPSO (Cloud
96 Aerosol Lidar and Infrared Pathfinder Satellite Observation) satellites are achieving notable
97 results by including a vertical dimension to traditional satellite data. CPR is a 94 GHz nadir-
98 looking radar. That is able to penetrate the optically thick clouds, while CALIOP is able to
99 detect tenuous cloud layer that are below the detection threshold of radar. In other words, it
100 has the ability to detect shallow clouds. Therefore, accurate location of cloud top and

complete vertical structure information of cloud can be obtained by the combined use of CPR and CALIOP, because of their unique complementary skills. Previous studies have shown that CloudSat/CALIPSO data are better accuracy compared with ISCCP and ground observation data (Sassen and Wang, 2008; Naud and Chen, 2010; Kim et al., 2011; Noh et al., 2011; Jiang et al., 2011). However, because the repeat time of these polar orbiting satellites for any particular location is very large, the time resolution of such observations is low (L'Ecuyer and Jiang, 2010; Qian et al., 2012). Both ground-based and space-based measurements have the problem of overlapping cloud layers that hide each other.

Some other methods have also been developed to detect cloud top heights from passive sensors. The CO₂-slicing method uses CO₂ differential absorption in the thermal infrared spectral range (Rossow and Schiffer, 1991; King et al., 1992; Platnick et al., 2003). Ultraviolet radiances can also be used as rotational Raman scattering causes depletion or filling of solar Fraunhofer lines in the UV spectrum, depending on the Rayleigh scattering above the cloud (Joiner and Bhartia, 1995; de Beek et al., 2001). Similarly, the polarization of reflected light, at visible shorter wavelength, due to Rayleigh scattering carries information on cloud top height (Goloub et al., 1994; Knibbe et al., 2000). Finally, cloud top height can also be retrieved by applying geometrical methods to stereo observations (Moroney et al., 2002; Seiz et al., 2007; Wu et al., 2009). Global Navigation Satellite System (GNSS) Radio Occultation (RO) profiles were used to detect the convective cloud top heights (Biondi et al., 2013). Recently, Biondi et al. (2017) used GNSS RO profiles to detect the top altitude of volcanic clouds and analyzed their impact on thermal structure of UTLS. Multi-angle and bi-spectral measurements in the O₂ A-band were used to derive the cloud top altitude and cloud geometrical thickness (Merlin et al., 2016 and references therein). However, this method is restricted to homogeneous plane-parallel clouds. For heterogeneous clouds or when aerosols lay above the clouds the spectra of reflected sunlight in the O₂ A-band will get modified.

An indirect way to perform estimations of CVS is by using atmospheric thermodynamic profiles measured by radiosondes. Radiosondes can penetrate atmospheric (and cloud) layers to provide in situ data. The profiles of temperature, relative humidity and pressure measured by radiosondes provide information about the CVS by identifying saturated levels in the atmosphere (Zhang et al., 2010). In fact, radiosonde measurements were probably the best measurements for deriving CVS from the ground (Wang et al., 2000; Eresmaa et al., 2006; Zhang et al., 2010). Very recently, George et al. (2018) provided CVS over India during depression (D) and non-depression (ND) events during South West monsoon season (July 2016) using one month of campaign data. However, detailed CVS in all the seasons including diurnal variation over Indian region is not made so far to the best of our knowledge.

The objective of this study is to examine the temperature structure of UTLS region during the occurrence of single-layer and multi-layer clouds over Gadanki location (13.5° N, 79.2° E). In the first, we focus to report the CVS using long-term (11 years) high vertical resolution radiosondes observations. The paper is organized as follows: data and methodology are described in Section 2. In Section 3, background weather conditions during the period of analysis are described. Results and discussion are given in Section 4. Finally, the summary and major conclusion drawn from the present study is provided in Section 5.

2. Data and Methodology

2.1. Data

In this study, long-term (11 years) observations of high vertical resolution radiosonde (Vaisälä RS-80, RS-92; Meisei RS-01GII, RS-6G, RS-11G, IMS-100) data are used to analyze CVS over a tropical station, Gadanki. There is no significant change in the accuracies of the meteorological parameters from these different radiosonde makes. Most of these radiosondes were launched around 1730 Local Time, LT (LT=UT+0530 h). In general, the balloons are not launched during moderate to heavy rain conditions. However, we have done

visual inspection of each radiosonde profile. The RH profiles which show continuous saturation with height were discarded. Figure 1 shows the monthly percentage of radiosonde data available from Apr. 2006 to May 2017. Total 3313 launches were made, out of which 98.9% and 86.6% reached altitudes greater than 12.5 km and 20 km, respectively. The data which have balloon burst altitude less than 12.5 km (1.1%) are discarded. Also, we have put condition on number of profiles in a month should be more than seven to represent that month. After applying these two conditions the total number of profiles was 3251. In addition, to study the diurnal variations in CVS over Gadanki, we made use of radiosonde observations taken from Tropical Tropopause Dynamics (TTD) campaigns (Venkat Ratnam et al., 2014b) conducted during Climate and Weather of Sun Earth Systems (CAWSES) India Phase II program (Pallamraju et al., 2014). During these campaigns, the radiosondes were launched every three hours for continuous three days in each month from Dec. 2010 to Mar. 2014 except in Dec. 2012, Jan., Feb., Apr., 2013.

2.2. Methodology

Several methods are employed to determine the CVS from the profiles of radiosonde data (Poore et al., 1995; Wang and Rossow, 1995; Chernykh and Eskridge, 1996; Minnis et al., 2005; Zhang et al., 2010). Poore et al. (1995) estimated the cloud base and cloud top using temperature-dependent dew-point depression thresholds. First, the dew-point depression must be calculated at every radiosonde level. According to Poore et al. (1995), a given atmospheric level has a cloud if $\Delta T_d < 1.7^\circ\text{C}$ at $T > 0^\circ\text{C}$, $\Delta T_d < 3.4^\circ\text{C}$ at $0 > T > -20^\circ\text{C}$, $\Delta T_d < 5.2^\circ\text{C}$ at $T < -20^\circ\text{C}$.

Wang and Rossow (1995) used the temperature, pressure and RH profiles and computed RH with respect to ice instead of liquid water for the levels with temperatures lower than 0°C . To this new RH profile they have applied two RH thresholds (min RH = 84% and max RH = 87%). In addition, if RH at the base (top) of the moist layer is lower than 84%, a RH jump

exceeding 3% must exist from the underlying (above) level. According to the Chernykh and Eskridge (1996) method, the necessary condition for the existence of clouds in a given atmospheric level is that the second derivatives with respect to height (z) of temperature and RH to be positive and negative, respectively ie., $T''(z) \geq 0$ and $RH''(z) \leq 0$. Minnis et al. (2005) provided an empirical parameterization that calculates the probability of occurrence of a cloud layer using RH and air temperature from radiosondes. First, RH values must be converted to RH with respect to ice when temperature is less than -20°C . Second, the profile has to be interpolated every 25 hPa up to the height of 100 hPa. An expression to estimate the cloud probability (P_{cld}) as a function of temperature and RH is then applied. In this expression, RH is given the maximum influence as it is the most important factor in cloud formation. Finally, a cloud layer is set wherever $P_{\text{cld}} \geq 67\%$. The Zhang et al. (2010) method is an improvement on the Wang and Rossow (1995) method. Instead of a single RH threshold, Zhang et al. (2010) applied altitude-dependent thresholds without the requirement of the 3% RH jump at the cloud base and top.

Costa-Suros et al. (2014) compared the CVS derived from these five methods described above by using 193 radiosonde profiles acquired at the Atmospheric Radiation Measurement (ARM) Southern Great Plains site during all seasons of the year 2009. The performance of the five methods has been assessed by comparing with Active Remote Sensing of Clouds (ARSCL) data taken as a reference. Costa-Suros et al. (2014) concluded that three of the methods (Poore et al., 1995; Wang and Rossow, 1995; and Zhang et al., 2010) perform reasonably well, giving perfect agreements for 50% of the cases and approximate agreements for 30% of the cases. The other methods gave poor results (lower perfect and/or approximate agreement, and higher false positive, false negative or not coincident detections). Among the three methods, Zhang et al. (2010) method is the most recent version of the treatment initially proposed in Poore et al. (1995) and Wang and Rossow (1995), and provides good results (a

perfect agreement of 53.9% and an approximate agreement of 29.5%). Thus, the algorithm of Zhang et al. (2010) is used for detecting cloud layers in our analysis.

Cloud layers are associated with high RH values above some threshold as the radiosonde penetrates through them. Cloud detection algorithm of Zhang et al. (2010) employs three height-resolving RH thresholds to determine cloud layers: minimum and maximum RH thresholds in cloud layers (min-RH and max-RH), and minimum RH thresholds within the distance of two adjacent layers (inter-RH). The height-resolving thresholds of max-RH, min-RH, and inter-RH values are specified in Table 1. The algorithm begins by converting RH with respect to liquid water to RH with respect to ice at temperatures below 0° C (see example in Figure 2). The accuracy of RH measurement is less than 5% up to the altitude 12.5 km and hence the RH profile is examined from the surface to 12.5 km (~ 200 hPa) altitude to find cloud layers in seven steps: (1) the base of the lowest moist layer is determined as the level when RH exceeds the min-RH corresponding to this level; (2) above the base of the moist layer, contiguous levels with RH over the corresponding min-RH are treated as the same layer; (3) the top of the moist layer is identified when RH decreases to that below the corresponding min-RH or RH is over the corresponding min-RH but the top of the profile is reached; (4) moist layers with bases lower than 500 m AGL (Above Ground Level) and thickness less than 400 m are discarded; (5) the moist layer is classified as a cloud layer if the maximum RH within this layer is greater than the corresponding max-RH at the base of this moist layer; (6) two contiguous layers are considered as a one-layer cloud if the distance between these two layers is less than 300 m or the minimum RH within this distance is more than the maximum inter-RH value within this distance; and (7) clouds are discarded if their thicknesses are less than 100 m.

At measurement location, we have Boundary Layer Lidar and Mie Lidar. When there is occurrence of multi-layer configuration, BLL does not give accurate cloud base altitude for

higher layers. Whereas, Mie LIDAR gives the vertical structure of the cirrus clouds (usually occur at higher altitude). Here, CVS is examined only up to 12.5 km altitude as the accuracy in RH measurements is poor at higher altitudes. Also, Mie LIDAR is operated mostly during cloud free conditions (only during cirrus cloud or clear sky conditions). Further, the timings of Radiosonde and LIDAR measurements are different. Therefore, we did not compare with the ground-based LIDAR measurements. On the other hand, CLOUDSAT/CALIPSO overpasses over experiment location are around 02 LT and 14 LT. Whereas regular radiosonde launches are around 1730 LT. Therefore, we did not compare the CVS derived from regular radiosonde and CLOUDSAT/CALIPSO measurements. However, we have three hourly radiosonde observations for continuous three days in every month during TTD campaigns. We did not get collocated (space and time) measurements from CLOUDSAT/CALIPSO and Radiosonde during these campaigns.

Before proceeding further, it is desired to verify the identified layers of clouds are correct or not with independent observations. For that we have launched Cloud Particle Sensor (CPS) sonde (Fujiwara et al., 2016) at Gadanki, which provides profile of cloud number concentration. Results from a flight of RS-11G radiosonde and Cloud Particle Sensor (CPS) Sonde on the same balloon launched at 02 LT on 04 Aug. 2017 at Gadanki, India is shown in Figure 2. Sudden increase in the cloud number concentration within the detected cloud layers indicates the cloud layer boundaries detected in the present study are in good agreement.

The drawback of using the radiosonde data for detecting the CVS at a given location is the radiosonde horizontal displacement, due to the drift produced by the wind. However, irrespective of the season, the maximum horizontal drift of radiosonde when it reaches the 12.5 km altitude is always less than 20 km (Venkat Ratnam et al., 2014a). One may expect different background features within this 20 km particularly the localised convection that may influence the CVS. In order to assess this aspect, we used outgoing longwave radiation

(OLR) as a proxy for tropical convection. Figure 3(a-d) shows the seasonal mean distribution of OLR (from KALPANA-1 satellite) around Gadanki location obtained during pre-monsoon, monsoon, post-monsoon and, winter seasons averaged during 2006 – 2017. It can be noted that irrespective of the season, homogeneous cloudiness prevailed for more than 50 km radius around Gadanki location. Hence, the CVS detected from the radiosonde can be treated as representative of Gadanki location.

Methodology described in Section 2.2 to detect CVS is applied on high vertical resolution radiosonde data acquired during Apr. 2006 to May 2017 from Gadanki, as well as special radiosondes launches during TTD campaigns from Oct. 2010 to Apr. 2014. Results are presented in Section 4. Before going further, it is desirable to examine the background meteorological conditions prevailing over Gadanki during different seasons.

3. Background meteorological conditions

National Atmospheric Research Laboratory (NARL) at Gadanki is located about 120 km northwest of Chennai (Madras) on the east coast of the southern Indian peninsula. This station is surrounded by hills with a maximum altitude of 350–400 m above the station, and the station is at an altitude of 375 m a.m.s.l. (hereinafter all altitudes are mentioned above mean sea level). The local topography is complex with a number of small hillocks around and a high hill of ~1 km about 30 km from the balloon launching site in the northeast direction. The detailed topography of Gadanki is shown in Basha and Ratnam (2009). Gadanki receives about 53% of the annual rainfall during the southwest monsoon (Jun. to Sep.) and 33% of the annual rainfall during the northeast monsoon (Oct. to Dec.) (Rao et al., 2008a). The rainfall during the southwest monsoon occurs predominantly from the evening to mid-night period. About 66% of total rainfall is convective in nature, while the remaining rain is widespread stratiform in character (Rao et al., 2008a).

Background meteorological conditions prevailing over the observational site are briefly described based on the radiosonde data collected during Apr. 2006 to May 2017. The seasons are classified as winter (December-January- February), pre-monsoon (March-April-May), monsoon (June-July-August-September), and post-monsoon (October-November). The climatological monthly mean contours of the temperature anomalies, relative humidity, zonal and meridional winds are shown in Figure 4(a–d), respectively. From surface to 1 km altitude, temperature anomalies show seasonal variability with warmer temperatures during pre-monsoon months and relatively lower temperatures during winter season (Figure 4a). Temperature anomalies do not show significant seasonal variation from 1 km altitude to the middle troposphere, but significant seasonal differences are observed in the lower stratosphere. There exist significant seasonal variations in the RH (Figure 4b). During winter, RH is small (40 – 50%) from surface to ~ 3 km altitude and is almost negligible above. However, during the other seasons, particularly in the peak monsoon months (Jul. and Aug.), large RH values (60–70%) are noticed up to 10 km altitude.

During winter, easterlies are observed up to 4–6 km altitude and westerlies above (Figure 4c). There seem to be weak easterlies between 14–20 km altitude during the pre-monsoon. During the monsoon season low level westerlies exist below 7–8 km and easterlies above. The Tropical Easterly Jet (TEJ) is prevalent over this region in the SW monsoon season, with peak velocity sometimes reaching more than 40 ms^{-1} (Roja Raman et al., 2009). There exist large vertical shears during monsoon in the zonal wind. Easterlies exist up to 20 km altitude during post-monsoon season. In general, meridional velocities are very small and are northerlies are observed up to 8 km and southerlies above in all the seasons, except during monsoon (Figure 4d). During the winter and monsoon, relatively stronger southerlies and northerlies prevailed, respectively, between 12 and 15 km altitudes. A clear annual oscillation can be noticed in both zonal and meridional velocities. Similar variations are also observed

by the MST radar located at the same site in between 4 and 20 km (Ratnam et al., 2008; Basha and Ratnam, 2009; Debashis Nath et al., 2009). Monthly mean OLR around Gadanki at 1730 LT is shown in Figure 4e. Low values of OLR ($< 220 \text{ W m}^{-2}$) around Gadanki location indicate that the occurrence of very deep convection during the monsoon season, consistent with the occurrence of high RH values up to 10 km altitude during monsoon season (Figure 4b).

4. Results

By adopting the methodology described in Section 2.2 we have detected a total of 4309 Cloud layers from 3251 radiosonde launches at Gadanki location during the period of data analysis. For each season, cloud layers during Apr. 2006 – May 2017 are averaged to obtain the composite picture of CVS. Seasonal variability in cloud layers is discussed in Section 4.2.

4.1. Diurnal variation of single-layer and multi-layer clouds

There are studies on the diurnal variation of cloud layers outside the Indian region. For example, over Porto Santo Island during the Atlantic Stratocumulus Transition Experiment (ASTEX) by Wang et al. (1999), over San Nicolas Island during First ISCCP Regional Experiment (FIRE) by Blaskovic et al. (1990), Over Shouxian (32.56° N , 116.78° E) location by Zhang et al. (2010). As per authors knowledge there are no studies on diurnal variability of cloud layers over Indian region. For the first time, over Indian land region, the diurnal variability of cloud layers are studied by using radiosonde observations taken from TTD campaigns. Figure 5(a-d) describes the diurnal variations of single-layer and multi-layer clouds during pre-monsoon, monsoon, post-monsoon, and winter seasons over Gadanki region. As mentioned in Section 2.1, from Dec. 2010 to Mar. 2014, we have launched radiosondes every three hourly for continuous three days in every month except during Dec. 2012, Jan., Feb., Apr., 2013. The total number of profiles taken during pre-monsoon, monsoon, post-monsoon, and winter seasons are 160, 254, 101, and 199, respectively.

Among these the number of cloudy profiles are 93 in pre-monsoon, 241 in monsoon, 63 in post-monsoon, and 96 in winter seasons.

From the Figure 5(a-d), for four seasons, diurnal variations of cloud occurrence show a maximum between 23 and 05 LT and a minimum at 14 LT, except during monsoon season. During monsoon season, a minimum in cloud occurrence occurred at 11 LT. Using Infrared Brightness temperature data over Indian region Gambheer and Bhat (2001), Zuidema (2003), Reddy and Rao (2018) observed the maximum frequency of occurrence of clouds during late night early morning hours. Percentage occurrence of one-layer and multi-layer clouds shows noticeable diurnal variations in all seasons except in monsoon season. Maximum percentage occurrence in one-layer clouds is at 08 LT in pre-monsoon season and it is at 17 LT during post-monsoon and winter seasons. For all the seasons, the maximum percentage occurrence in multi-layer clouds is between 20 and 05 LT. Figure 6(a-d) describes the mean vertical locations (base and top) and cloud thicknesses of one-layer clouds during pre-monsoon, monsoon, post-monsoon, and winter seasons, respectively. During monsoon season, the maximum in cloud top altitude is at 05 LT and minimum is at 14 LT (Figure 6(b)). In general, cloud base of one-layer cloud occur at higher altitude between 11 and 14 LT and it occur relatively low altitudes between 20 and 08 LT. Except during post-monsoon season, the single-layer clouds are high-level clouds with base is greater than 5 km most of the times. During post-monsoon season, the single-layer clouds are low-level at 05 LT (cloud-base altitude of 1.4 km) and middle level-clouds between 14 and 02 LT (Figure 6c). During pre-monsoon and monsoon seasons, thickness of single-layer clouds reaching a maximum at 23 LT and a minimum at 14 LT (Figure 6(a-b)). The minimum in one-layer cloud thickness at 14 LT is due to the increase of cloud base altitude and simultaneous decrease of cloud top altitude. There is not much variability in thickness of one-layer clouds during post-monsoon and winter seasons (Figure 6(c-d)). Figure 7(a-d) and Figure S1(a-d) are same as Figure 6(a-

d) but for two-layer and three-layer clouds. Similar to one-layer cloud, the cloud base of bottom-layer of two-layer clouds show maximum between 11 and 14 LT and minimum between 20 and 08 LT. Thickness of top layer and bottom layer of two-layer clouds reaching a minimum value between 11 and 14 LT. Upper layer of two-layer clouds show a maximum in thickness at 23 LT and minimum at 11 LT during monsoon season (Figure 7(b)).

The cloud maintenance and development are strongly modulated by diabatic processes, namely solar heating and longwave (LW) radiative cooling (Zhang et al., 2010). Near noontime (11 - 14 LT), solar heating is so strong that (1) evaporation of cloud drops may occur and (2) atmospheric stability may increase thus suppressing cloud development. So near noontime, the vertical development of single-layer clouds and the vertical development of the uppermost layer of multiple layers of cloud are suppressed due to solar heating. This effect is predominant during monsoon season for one-layer and two-layer clouds (Figures 6(b) and 7(b)), during pre-monsoon and post-monsoon seasons for three-layer clouds (Figures S1a and S1c). However, for lower layers of cloud in a multiple-layer cloud configuration, solar heating is greatly reduced because of the absorption and scattering processes of the upper layers of cloud. In general maximum in surface temperature occurs around 15:20 LT (Reddy and Rao, 2018). The ground surface is warmer than any cloud layer so through the exchange of LW radiation, the cloud base gains more energy. This facilitates cloud development and leads to a maximum in cloud altitude and thickness between 14 and 17 LT (Figures 7a, 7b, 7d and S1a). This effect is predominant during winter season for two layer clouds (Figure 7d) and during pre-monsoon season for three-layer clouds (Figure S1a). As the sun sets, LW radiative cooling starts to dominate over shortwave (SW) radiative warming. Cloud top temperatures begin to lower, which increases atmospheric instability and fuels the development of single-layer clouds and the uppermost layer of cloud in multiple-layer cloud configurations. At sunset, solar heating diminishes and LW cooling strengthens, which may

explain why there is a peak between 20 and 23 LT in the thickness of one-layer clouds and the uppermost layer of two-layer cloud. This effect is clearly observed in the monsoon season (Figures 6b, 7b, S1b). We conclude that diurnal variability in base, top and thickness for single-layer, two-layer and, three-layer clouds are significant. Hence there can be a bias in cloud vertical structure when we are studying the composite over a season by using polar satellites.

Next Section, we show the seasonal variability in cloud layers using long-term (11 years) observations of high vertical resolution radiosonde over Gadanki. Note that most of these radiosondes were launched around 1730 LT hence there will be bias in the results due to diurnal variability of cloud layers which we have discussed above. Hence the results related to seasonal variability of cloud layers are only representative of 1730 LT.

4.2. Seasonal variability in the cloud layers

Figure 8(a-c) describes the percentage occurrence of base, top and thickness of cloud layers observed during different seasons over Gadanki. The cloud base altitude shows a bimodal distribution in all seasons except during pre-monsoon season (Figure 8a). During pre-monsoon season, the peak of cloud base altitude distribution is observed at ~6.2 km (~7.5%). During other three seasons (monsoon, post-monsoon and winter), the first peak in cloud base altitude is observed between 2 and 3 km altitude region and the second peak is observed at ~6.2 km. Using CLOUDSAT observations over the Indian monsoon region, Das et al. (2017) also reported that the cloud base altitude over Indian monsoon region shows a bimodal distribution. However, the first peak in cloud base altitude is observed at ~14 km while the second maximum is at 2 km.

The cloud top altitude increases above 12 km altitude and have a maximum at 12.5 km in all seasons (Figure 8b). Note that we restrict maximum altitude as 12.5 km due to limitation in providing reliable water vapor above that altitude from normal radiosondes. At lower

altitudes, during the monsoon season the peak in cloud top altitude is at 2.9 km and it increases to 3.3 km during the post-monsoon season. However we have also checked the cloud vertical structure till 18 km. There is no significant difference in the cloud base and cloud top altitude distribution (See Figure S2). Das et al. (2017) reported that there are two peaks in the cloud top altitude; one at ~17 km and other is at ~3 km. The peaks in cloud base and cloud top at higher altitudes as observed by Das et al. (2017) could be due to the occurrence of cirrus clouds.

The cloud base altitude values are subtracted from the cloud top altitude for each cloud layer to extract the cloud thickness. Figure 8(c) describes the percentage occurrence of the cloud thickness observed during different seasons. The occurrence of thicker clouds decreases exponentially. The cloud thickness has a maximum below 500 m for all seasons, which constituted about 34.7%, 26.5%, 31.2% and 36.6% of the total observed cloud layers during pre-monsoon, monsoon, post-monsoon and winter seasons, respectively. In general, for all seasons, more than 65% of clouds layers have cloud thickness < 2 km.

Different cloud types occurring at different height regions have a spectrum of effects on the radiation budget (Behrangi et al., 2012). Therefore, the clouds have been classified into four groups based on the cloud base altitude and their thickness (Lazarus et al., 2000 and Zhang et al., 2010): (1) low-level clouds with bases lower than 2 km and thickness less than 6 km; (2) middle-level clouds with bases ranging from 2 to 5 km; (3) high-level clouds with bases greater than 5 km; and (4) deep convective cloud (hereafter called DCC) with base less than 2 km and thicknesses greater than 6 km. These four types of clouds account for 11.97%, 26.71%, 59.36% and 1.95% of all cloudy cases, respectively. Figure 9(a-d) describe the mean vertical locations (base and top), cloud thicknesses and percentage occurrence of low-, middle-, high-level clouds, and DCC observed during different seasons. At Gadanki location, there is a distinct persistence of the high-level clouds over all the seasons. The occurrence of

the high-level clouds is 69.05%, 58.49%, 55.5%, and 58.6% during the pre-monsoon, monsoon, post-monsoon, and winter seasons, respectively (Figure 9c). In general, after the dissipation of deep convective clouds they spread large anvils and remain persist as high level clouds for longer duration. These high level clouds could be due to in-situ generated Convective Systems or else propagated from the surrounding Oceans. Zuidema (2003) reported that the deep convective systems generated over central and west Bay of Bengal (BoB) advect toward the inland region of southern peninsular India and dissipates. In general, the high level clouds follow background winds at those levels. Especially during monsoon season, due to the strong westerly winds in the upper levels, high level clouds which are originated from MCS over BoB advect into the Indian land region and contribute to the high level cloud occurrence. Hence the outflow caused by the deep convective systems could be responsible for the higher percentage occurrence of high-level clouds. The low-level (middle-level) clouds contribute about 3.74%, 10.45%, 16.27%, and 20.89% (27.04%, 29.35%, 24.28%, and 18.67%) of all cloudy cases during the pre-monsoon, monsoon, post-monsoon, and winter seasons, respectively (Figure 9a-b).

Thicknesses of low-, middle-, and high-level clouds has minimum values during winter season and maximum values in monsoon season (Figure 9a-c). Whereas DCC have minimum thickness in winter and maximum in pre-monsoon season (Figure 9d). The average cloud base (cloud top) altitudes for low-, middle-, and high-level clouds and deep convective clouds are 1.74 km (3.16 km), 3.59 km (5.55 km), 8.79 km (10.49 km), and 1.22 km (11.45 km), respectively. Over Indian summer monsoon region, Das et al. (2017) reported that the percentage occurrence of high-level clouds is more than the other three cloud types. Over Shouxian (32.56° N, 116.78° E) location, Zhang et al. (2010) reported that the percentage occurrence of low-, middle-, high-level clouds and deep convective clouds is 20.1%, 19.3%, 59.5%, and 1.1%, respectively.

4.2.1. Single-layer and Multi-layer clouds

By interacting with both shortwave and longwave radiation, clouds play crucial role in the radiative budget at the surface, within and at the top of the atmosphere. Over the tropics, the zonal mean net cloud radiative effect differences between multi-layer clouds and single-layer clouds were positive and dominated by the shortwave cloud radiative effect differences (Li et al., 2011). This is because, the multi-layer clouds reflect less sunlight to the top of the atmosphere and transmit more to the surface and within the atmosphere than the single-layer clouds as a whole. As a result, multi-layer clouds warm the earth-atmosphere system when compared to single-layer clouds (Li et al., 2011). In this study, we studied the occurrence of single-layer and multi-layer clouds obtained during different seasons at Gadanki location. The percentage occurrence of single-layer, two-layer, three-layer and four- or more- layer clouds during pre-monsoon, monsoon, post-monsoon and winter seasons are shown in Figure 10(a-d). Single-layer, two-layer and three-layer clouds account for 40.80%, 30.71%, and 19.68% of all cloud configurations, respectively. Even though the low frequency of occurrence of one-layer clouds over Gadanki, they exhibit pronounced seasonal variation in magnitude with very low frequency during pre-monsoon season. This may be due to the strong warm and dry atmospheric conditions from surface to boundary layer top (Figure 4a and 4b). Percentage occurrence of single-layer (multi-layer) clouds during pre-monsoon, monsoon, post-monsoon and winter seasons are 7.7%, 14.2%, 8.48% and 10.42% (7.93%, 34.58%, 10.83% and 5.86%), respectively. There is a significant occurrence of multi-layer clouds during monsoon season than other seasons indicating that the development of multi-layer clouds is favorable under warm and moist atmospheric conditions (Figures 4a and 4b). Among the different cloud layers, the two-layer clouds have maximum percentage occurrence (16.6%) during monsoon season (Figure 10b). Luo et al. (2009) reported the occurrence of multi-layer clouds over the Indian region during the summer season and attributed it to the

complex cloud structure associated with the monsoon system. Zhang et al. (2010) reported that multi-layer cloud occurrence frequency is relatively higher during summer months (Jun., Jul. and Aug.) than autumn months (Sep., Oct. and Nov.) over Shouxian. Recently, Using the four years of combined observations of Cloudsat and CALIPSO, Subrahmanyam and Kumar (2017) reported the maximum frequency of occurrence of two-layer clouds over Indian sub-continent during Jun. Jul. and Aug months. This they attributed to the presence of Indian summer monsoon circulation over this region, which is dominated by the formation of various kinds of clouds such as cumulus, stratocumulus, cirrus etc.,. Very recently, George et al. (2018) reported CVS using the radiosonde launches during depression (D) and non-depression (ND) events in South West monsoon season using one month of field campaign data over Kanpur, India.

Figure 11(a-c) describe the mean vertical locations (base and top) and cloud thicknesses of single-layer, two-layer and three-layer clouds during different seasons. Except during winter season, single-layer clouds are thicker than the layers forming multi-layer clouds. Also, upper layer clouds are thicker than lower layer clouds in multi-layer clouds. This could be due to the exchange of longwave radiation between cloud base of upper layer and cloud top of lower layer. As a result, the strong reduction in longwave radiation cooling at the top of the lower layer of cloud in the presence of upper layers of cloud (Zhang et al., 2010; Wang et al., 1999; Chen and Cotton, 1987).

Irrespective of the season, single-layer clouds are high-level clouds i.e cloud base is > 5 km (Figure 11a). Maximum cloud top altitude and the cloud thickness occurred during monsoon season for single-layer clouds (Figure 11a) and the uppermost layer of multi-layer cloud configurations (Figure 11b-c). This is consistent with the low OLR values ($< 220 \text{ W m}^{-2}$) observed during monsoon season (Figure 11d). Except during pre-monsoon season, cloud base, cloud top and cloud thickness values of lower layer of multi-layer clouds are

same during monsoon, post-monsoon and winter seasons. Whereas during pre-monsoon season, cloud base and cloud top of lower layer of multi-layer clouds occurred at relatively higher altitudes (Figure 11b-c). Similarly, there are no significant variations in cloud thickness in middle layer of three-layer clouds between the seasons. However, cloud base and cloud top of middle layer of three-layer clouds during pre-monsoon season occurred relatively at higher altitudes than the other three seasons (Figure 11c). Table 2 describes the mean base, top and thicknesses of cloud layers of single-layer, two-layer and three-layer clouds. In the two-layer clouds, the thickness of the upper level cloud layer is about the same as those of single-layer clouds. In the three-layer clouds, the base and top heights of the lowest layer of cloud are similar to those of the lowest layer of cloud in two-layer clouds.

4.3. Variability in CVS with respect to SW monsoon arrival over Gadanki

CVS play an important role in the summer monsoon because they can significantly affect the atmospheric heat balance through latent heating caused by water phase changes and through scattering of radiation. In this Section we discuss the variability in different clouds with respect to the date of arrival of southwest (SW) monsoon over Gadanki. SW monsoon onset occurs over Kerala coast (south west coast of India) during the last week of the May or first week of June. In general, the climatological mean monsoon onset over Kerala (MOK) is on 1 June with ± 7 days. It is to be noted that the climatology onset date is obtained from IMD long term onset dates and arrival date over Gadanki is picked up manually from the yearly onset date lines over India map given by IMD.

Figure 12 shows the composite (2006 – 2016) percentage occurrence of clear sky and cloud days (Figure 12a), low-level, middle-level, high-level and deep convective clouds (Figure 12b), and one-, two-, three- and four or more- layer clouds (Figure 12c) with respect to monsoon arrival date. Figures 13(a-c) describe the mean vertical locations (base and top) and cloud thicknesses of single-layer, two-layer clouds with respect to monsoon arrival date.

Day zero in Figures 12(a-b) and Figures 13(a-b) indicates the date of monsoon arrival over Gadanki location. The percentages occurrences of clear sky conditions prior to the monsoon arrival over Gadanki location decreases and reduce to zero on the date of monsoon arrival (Figure 12a). This indicates the estimated dates of monsoon arrival over Gadanki location are correct. From day four onwards the cloudiness start increases and peaks on day 18 (Figure 12a). The percentage occurrence of middle level clouds decreases till 5 days prior to the monsoon arrival (Figure 12b). Subsequently middle level clouds percentage increases and does not show significant variability later to the monsoon arrival. There are no deep convective clouds prior and during the monsoon arrival over Gadanki location (Figure 12b). They occurred on day 3, 9, 10, 17 and 20. During and later to the arrival of the monsoon, the percentage occurrence of multilayer clouds is always greater than the single layer clouds except day three and four (Figure 12c). Day zero it is noted that single layer clouds are high level clouds and they are thicker with thickness ~ 6.7 km (Figure 13a). In two layer clouds the bottom layer is middle layer cloud and top layer is high level cloud (Figure 13b). The bottom layer is thicker than the top layer. During deep convective clouds and middle level, single layer clouds prevailed. The thickness of single layer clouds show large variability with thickness ranging from 300 m to 5 km during the first week later to the arrival of the monsoon. In the second week, the thickness ranges from 2 km to 5 km (Figure 13a). Later to the arrival of the monsoon, thickness of bottom layer in two layer cloud is relatively higher than the top layer (Figure 13b). Thicker single layer clouds and bottom layer of two layer clouds later to the monsoon arrival over Gadanki is due to the increase of tropospheric water vapor.

5. Summary

Cloud vertical structure (CVS) is studied for the first time over India by using long-term high vertical resolution radiosonde measurements at Gadanki location obtained during Apr.

2006 to May 2017. In order to obtain diurnal variation in CVS, we have used 3 hourly launched radiosondes for 3 days in each month during Dec. 2010 to Mar. 2014. CVS is obtained following Zhang et al. (2010) where it relay on height-resolved relative humidity thresholds. After obtaining the cloud layers they are segregated to low, middle and high level clouds depending upon their altitude of occurrence. Detected layers are verified using independent measurements from cloud particle sensor (CPS) sonde launched from same location. Very good match between these two independent measurements is noticed.

First, the diurnal variations in CVS over Gadanki is studied using radiosonde observations taken from TTD campaigns conducted during CAWSES India Phase II program. During pre-monsoon and monsoon seasons, thickness of single-layer clouds reaches a maximum at 23 LT and a minimum at 14 LT. Upper layer of two-layer clouds show a maximum in thickness at 23 LT and minimum at 11 LT during monsoon season. Radiosonde measurements around 1730 LT were used to study the seasonal variability in CVS. After ascertaining the cloud layers they are segregated into different season to obtain the season variation of CVS. High-level clouds account for 69.05%, 58.49%, 55.5%, and 58.6% of cloud layers identified during pre-monsoon, monsoon, post-monsoon, and winter seasons, respectively, indicating high cloud layers being most prevalent at Gadanki location. Single-layer, two-layer, and three-layer clouds account for 40.80%, 30.71%, and 19.68% of all cloud configurations, respectively. Multi-layer clouds occurred more frequently during the monsoon with 34.58%. Maximum cloud top altitude and the cloud thickness occurred during monsoon season for single-layer clouds and the uppermost layer of multi-layer cloud configurations.

Further, we have discussed the variability in different clouds with respect to the date of arrival of southwest (SW) monsoon over Gadanki location. Prior, during and later to the SW monsoon arrival over Gadanki location, high level clouds occurrence is more than the other

cloud types. Whereas the middle level cloud occurrence decreases till 5 days prior to the monsoon arrival and increases subsequently. There are no deep convective clouds prior and during the monsoon arrival over Gadanki location. The thickness of single layer clouds shows large variability during the first week later to the arrival of the monsoon. But it increases significantly between 8 and 11 days later to the monsoon arrival. Later to the arrival of the monsoon, thickness of bottom layer in two layer cloud is relatively higher than the top layer. Thicker single layer clouds and bottom layer of two layer clouds later to the monsoon arrival over Gadanki is due to the increase of tropospheric water vapor.

These cloud layers are expected to affect significantly to the background temperature in the troposphere and lower stratosphere. The composite (2006-2016) temperature profiles during clear sky, one-layer, two-layer, three-layer and four or more-layer cloud occurrences are shown in Figure 14. The temperature differences between the cloudy (single-, two-, three-, four or more- layer) and clear sky conditions are shown with dash lines in Figure 14. The striking result here is that occurrence of peak cooling (peak warming) below (above) the Cold Point Tropopause (CPT) altitude. The magnitude of cooling (warming) increases from single-layer to four or more-layer cloud occurrence. The peak cooling and warming during four or more-layer cloud occurrence are 0.9 K (at 15.7 km) and 3.6 K (at 18.1 K). Both single-layer and multi-layer clouds shows warming between 5 km and 14.5 km altitude region. The peak warming of 0.8 K at 9.5 km for single-layer cloud, and 1.3 K at 10.2 K for multi-layer clouds are observed and these altitudes are close to the cloud top altitude of single layer cloud and top layer of multi-layer clouds (Table 2). The detailed study on the impact of single-layer and multi-layer clouds on UTLS dynamics and thermodynamics structure will be investigated in our subsequent article including their radiative forcing.

Acknowledgements

We are grateful to the staffs of National Atmospheric Research Laboratory (NARL), Gadanki, who are involved in GPS radiosonde launching. Data used in the present study can be obtained on request. We thank associate editor and three anonymous reviewers for providing constructive comments/suggestions which made us to improve the manuscript content further.

References

Basha, G., Ratnam, M.V.: Moisture variability over Indian monsoon regions observed using high resolution radiosonde measurements. *Atmos. Res.* 132–133, 35–45. doi:10.1016/j.atmosres.2013.04.004, 2013.

Basha, G., Ratnam, M.V.: Identification of atmospheric boundary layer height over a tropical station using high-resolution radiosonde refractivity profiles: Comparison with GPS radio occultation measurements. *J. Geophys. Res. Atmos.* 114, D16101. doi:10.1029/2008JD011692, 2009.

Behrangi, A., Kubar, T., Lambrigtsen, B.: Phenomenological Description of Tropical Clouds Using CloudSat Cloud Classification. *Mon. Weather Rev.* 140, 3235–3249. doi:10.1175/MWR-D-11-00247.1, 2012.

Biondi, R., Randel, W. J., Ho, S.-P., Neubert, T. and Syndergaard, S.: Thermal structure of intense convective clouds derived from GPS radio occultations, *Atmos. Chem. Phys.*, 12(12), 5309–5318, doi:10.5194/acp-12-5309-2012, 2012.

Biondi, R., Ho, S.-P., Randel, W.J., Neubert, T., Syndergaard, S.: Tropical cyclone cloud-top height and vertical temperature structure detection using GPS radio occultation measurements. *J. Geophys. Res. Atmos.* 118, 5247–5259. doi:10.1002/jgrd.50448, 2013.

Biondi, R., Steiner, A. K., Kirchengast, G., Brenot, H. and Rieckh, T.: Supporting the detection and monitoring of volcanic clouds: A promising new application of Global

623 Navigation Satellite System radio occultation, *Adv. Sp. Res.*, 60(12), 2707–2722, doi:
624 10.1016/j.asr.2017.06.039, 2017.

625 Blaskovic, M., Davies, R., Snider, J.B.: Diurnal Variation of Marine Stratocumulus over San
626 Nicolas Island during July 1987. *Mon. Weather Rev.* 119, 1469–1478. doi:10.1175/1520-
627 0493(1991)119<1469:DVOMSO>2.0.CO;2, 1990.

628 Cesana, G., Chepfer, H.: How well do climate models simulate cloud vertical structure? A
629 comparison between CALIPSO-GOCCP satellite observations and CMIP5 models. *Geophys.*
630 *Res. Lett.* 39, n/a-n/a. doi:10.1029/2012GL053153, 2012.

631 Chahine, M.T., Pagano, T.S., Aumann, H.H., Atlas, R., Barnett, C., Blaisdell, J., Chen, L.,
632 Divakarla, M., Fetzer, E.J., Goldberg, M., Gautier, C., Granger, S., Hannon, S., Irion, F.W.,
633 Kakar, R., Kalnay, E., Lambrigtsen, B.H., Lee, S.-Y., Le Marshall, J., McMillan, W.W.,
634 McMillin, L., Olsen, E.T., Revercomb, H., Rosenkranz, P., Smith, W.L., Staelin, D., Strow,
635 L.L., Susskind, J., Tobin, D., Wolf, W., Zhou, L.: AIRS: Improving Weather Forecasting and
636 Providing New Data on Greenhouse Gases. *Bull. Am. Meteorol. Soc.* 87, 911–926.
637 doi:10.1175/BAMS-87-7-911, 2006.

638 Chen, C., Cotton, W.R.: The Physics of the Marine Stratocumulus-Capped Mixed Layer. *J.*
639 *Atmos. Sci.* 44, 2951–2977. doi:10.1175/1520-0469(1987)044<2951:TPOTMS>2.0.CO;2,
640 1987.

641 Chernykh, I. V, Eskridge, R.E.: Determination of Cloud Amount and Level from Radiosonde
642 Soundings. *J. Appl. Meteorol.* 35, 1362–1369. doi:10.1175/1520-
643 0450(1996)035<1362:DOCAAL>2.0.CO;2, 1996.

644 Costa-Surós, M., Calbó, J., González, J.A., Long, C.N.: Comparing the cloud vertical
645 structure derived from several methods based on radiosonde profiles and ground-based
646 remote sensing measurements. *Atmos. Meas. Tech.* 7, 2757–2773. doi:10.5194/amt-7-2757-
647 2014, 2014.

648 Crewell, S., Bloemink, H., Feijt, A., García, S.G., Jolivet, D., Krasnov, O.A., Van Lammeren,
 649 A., Löhnert, U., Van Meijgaard, E., Meywerk, J., Quante, M., Pfeilsticker, K., Schmidt, S.,
 650 Scholl, T., Simmer, C., Schröder, M., Trautmann, T., Venema, V., Wendisch, M., Willén, U.:
 651 THE BALTEX BRIDGE CAMPAIGN: An Integrated Approach for a Better Understanding
 652 of Clouds. *Bull. Am. Meteorol. Soc.* 85, 1565–1584. doi:10.1175/BAMS-85-10-1565, 2004.
 653 Das, S.K., Golhait, R.B., Uma, K.N.: Clouds vertical properties over the Northern
 654 Hemisphere monsoon regions from CloudSat-CALIPSO measurements. *Atmos. Res.* 183,
 655 73–83. doi:<https://doi.org/10.1016/j.atmosres.2016.08.011>, 2017.
 656 de Beek, R., Vountas, M., Rozanov, V. V., Richter, a., and Burrows, J. P.: The ring effect in
 657 the cloudy atmosphere, *Geophys. Res. Lett.*, 28, 721–724, doi:10.1029/2000GL012240,
 658 2001.
 659 Eresmaa, N., Karppinen, A., Joffre, S.M., Räsänen, J., Talvitie, H.: Mixing height
 660 determination by ceilometer. *Atmos. Chem. Phys.* 6, 1485–1493. doi:10.5194/acp-6-1485-
 661 2006, 2006.
 662 Fujiwara, M., Sugidachi, T., Arai, T., Shimizu, K., Hayashi, M., Noma, Y., Kawagita, H.,
 663 Sagara, K., Nakagawa, T., Okumura, S., Inai, Y., Shibata, T., Iwasaki, S., Shimizu, A.;
 664 Development of a cloud particle sensor for radiosonde sounding. *Atmos. Meas. Tech.* 9,
 665 5911–5931. doi:10.5194/amt-9-5911-2016, 2016.
 666 Gambheer, A. V, Bhat, G.S.: Diurnal variation of deep cloud systems over the Indian region
 667 using INSAT-1B pixel data. *Meteorol. Atmos. Phys.* 78, 215–225. doi:10.1007/s703-001-
 668 8175-4, 2001.
 669 George, G., Sarangi, C., Tripathi, S. N., Chakraborty, T., & Turner, A.: Vertical structure and
 670 radiative forcing of monsoon clouds over Kanpur during the 2016 INCOMPASS field
 671 campaign. *J. Geophys. Res.*, 123. <https://doi.org/10.1002/2017JD027759>, 2018.

672 Goloub, P., Deuze, J. L., Herman, M., and Fouquart, Y.: Analysis of the POLDER
 673 polarization measurements performed over cloud covers, *IEEE T. Geosci. Remote*, 32, 78–
 674 88, doi:10.1109/36.285191, 1994.

675 Hahn, C.J., Rossow, W.B., Warren, S.G.: ISCCP Cloud Properties Associated with Standard
 676 Cloud Types Identified in Individual Surface Observations. *J. Clim.* 14, 11–28.
 677 doi:10.1175/1520-0442(2001)014<0011:ICPAWS>2.0.CO;2, 2001.

678 Heintzenberg, J., Charlson, R.J. (Eds.): Clouds in the perturbed climate system: their
 679 relationship to energy balance, atmospheric dynamics and precipitation. MIT Press,
 680 Cambridge, UK, 2009.

681 Huang, Y.: On the Longwave Climate Feedbacks. *J. Clim.* 26, 7603–7610. doi:10.1175/JCLI-
 682 D-13-00025.1, 2013.

683 Jiang, X., Waliser, D.E., Li, J.-L., Woods, C.: Vertical cloud structures of the boreal summer
 684 intraseasonal variability based on CloudSat observations and ERA-interim reanalysis. *Clim.*
 685 *Dyn.* 36, 2219–2232. doi:10.1007/s00382-010-0853-8, 2011.

686 Joiner, J. and Bhartia, P. K.: The determination of cloud pressures from rotational Raman
 687 scattering in satellite backscatter ultraviolet measurements, *J. Geophys. Res.*, 100, 23019–
 688 23026, doi:10.1029/95JD02675, 1995.

689 Kim, S.-W., Chung, E.-S., Yoon, S.-C., Sohn, B.-J., Sugimoto, N.: Intercomparisons of
 690 cloud-top and cloud-base heights from ground-based Lidar, CloudSat and CALIPSO
 691 measurements. *Int. J. Remote Sens.* 32, 1179–1197. doi:10.1080/01431160903527439, 2011.

692 Lazarus, S.M., Krueger, S.K., Mace, G.G.: A Cloud Climatology of the Southern Great Plains
 693 ARM CART. *J. Clim.* 13, 1762–1775. doi:10.1175/1520-
 694 0442(2000)013<1762:ACCOTS>2.0.CO;2, 2000.

695 King, N. J. and Vaughan, G.: Using passive remote sensing to retrieve the vertical variation
696 of cloud droplet size in marine stratocumulus: An assessment of information content and the
697 potential for improved retrievals from hyperspectral measurements, *J. Geophys. Res.*, 117,
698 D15206, doi:10.1029/2012JD017896, 2012.

699 Knibbe, W. J. J., De Haan, J. F., Hovenier, J. W., Stam, D. M., Koelemeijer, R. B. A., and
700 Stammes, P.: Deriving terrestrial cloud top pressure from photopolarimetry of reflected light,
701 *J. Quant. Spectrosc. Ra.*, 64, 173–199, doi:10.1016/S0022-4073(98)00135-6, 2000.

702 L’Ecuyer, T. ~S., Jiang, J. ~H.: Touring the atmosphere aboard the A-Train. *Phys. Today* 63,
703 36. doi:10.1063/1.3463626, 2010.

704 Li, J., Yi, Y., Minnis, P., Huang, J., Yan, H., Ma, Y., Wang, W., Kirk Ayers, J.: Radiative
705 effect differences between multi-layered and single-layer clouds derived from CERES,
706 CALIPSO, and CloudSat data. *J. Quant. Spectrosc. Radiat. Transf.* 112, 361–375.
707 doi:https://doi.org/10.1016/j.jqsrt.2010.10.006, 2011.

708 Li, Y., Liu, X., Chen, B.: Cloud type climatology over the Tibetan Plateau: A comparison of
709 ISCCP and MODIS/TERRA measurements with surface observations. *Geophys. Res. Lett.*
710 33, n/a-n/a. doi:10.1029/2006GL026890, 2006.

711 Li, Z., Barker, H.W., Moreau, L.: The variable effect of clouds on atmospheric absorption of
712 solar radiation. *Nature* 376, 486–490, 1995.

713 Li, Z., Cribb, M.C., Chang, F.-L., Trishchenko, A., Luo, Y.: Natural variability and sampling
714 errors in solar radiation measurements for model validation over the Atmospheric Radiation
715 Measurement Southern Great Plains region. *J. Geophys. Res. Atmos.* 110, n/a-n/a.
716 doi:10.1029/2004JD005028, 2005.

717 Luo, Y., Zhang, R., Wang, H.: Comparing Occurrences and Vertical Structures of
718 Hydrometeors between Eastern China and the Indian Monsoon Region Using
719 CloudSat/CALIPSO Data. *J. Clim.* 22, 1052–1064. doi:10.1175/2008JCLI2606.1, 2009.

720 Merlin, G., Riedi, J., Labonnote, L. C., Cornet, C., Davis, A. B., Dubuisson, P., Desmons,
 721 M., Ferlay, N., and Parol, F.: Cloud information content analysis of multi-angular
 722 measurements in the oxygen A-band: application to 3MI and MSPI, *Atmos. Meas. Tech.*, 9,
 723 4977-4995, doi:amt-9-4977-2016, 2016.

724 Minnis, P., Yi, Y., Huang, J., Ayers, K.: Relationships between radiosonde and RUC-2
 725 meteorological conditions and cloud occurrence determined from ARM data. *J. Geophys.*
 726 *Res. Atmos.* 110, n/a-n/a. doi:10.1029/2005JD006005, 2005.

727 Moroney, C., Davies, R., and Muller, J.-P.: Operational retrieval of cloud-top heights using
 728 MISR data, *IEEE T. Geosci. Remote*, 40, 1532–1540, doi:10.1109/TGRS.2002.801150,
 729 2002.

730 Nath, D., Venkat Ratnam, M., Jagannadha Rao, V.V.M., Krishna Murthy, B. V, Vijaya
 731 Bhaskara Rao, S.: Gravity wave characteristics observed over a tropical station using high-
 732 resolution GPS radiosonde soundings. *J. Geophys. Res. Atmos.* 114, n/a-n/a.
 733 doi:10.1029/2008JD011056, 2009.

734 Naud, C.M., Chen, Y.-H.: Assessment of ISCCP cloudiness over the Tibetan Plateau using
 735 CloudSat-CALIPSO. *J. Geophys. Res. Atmos.* 115, n/a-n/a. doi:10.1029/2009JD013053,
 736 2010.

737 Naud, C.M., Muller, J.-P., Clothiaux, E.E.: Comparison between active sensor and
 738 radiosonde cloud boundaries over the ARM Southern Great Plains site. *J. Geophys. Res.*
 739 *Atmos.* 108, n/a-n/a. doi:10.1029/2002JD002887, 2003.

740 Noh, Y.-J., Seaman, C.J., Vonder Haar, T.H., Hudak, D.R., Rodriguez, P.: Comparisons and
 741 analyses of aircraft and satellite observations for wintertime mixed-phase clouds. *J. Geophys.*
 742 *Res. Atmos.* 116, n/a-n/a. doi:10.1029/2010JD015420, 2011.

743 Nowak, D., Ruffieux, D., Agnew, J.L., Vuilleumier, L.: Detection of Fog and Low Cloud
 744 Boundaries with Ground-Based Remote Sensing Systems. *J. Atmos. Ocean. Technol.* 25,

1357–1368. doi:10.1175/2007JTECHA950.1, 2008.

Pallamraju, D., Gurubaran, S., Venkat Ratnam, M.: A brief overview on the special issue on
CAWSES-India Phase II program. *J. Atmos. Solar-Terrestrial Phys.* 121, 141–144.
doi:<https://doi.org/10.1016/j.jastp.2014.10.013>, 2014.

Platnick, S., King, M. D., Ackerman, S., Menzel, W. P., Baum, B., Riedi, J. C., and Frey, R.:
The MODIS cloud products: Algorithms and examples from Terra, *IEEE T. Geosci. Remote*,
41, 459–473, doi:10.1109/TGRS.2002.808301, 2003.

Poore, K.D., Wang, J., Rossow, W.B.: Cloud Layer Thicknesses from a Combination of
Surface and Upper-Air Observations. *J. Clim.* 8, 550–568. doi:10.1175/1520-
0442(1995)008<0550:CLTFAC>2.0.CO;2, 1995.

Qian, Y., Long, C.N., Wang, H., Comstock, J.M., McFarlane, S.A., Xie, S.: Evaluation of
cloud fraction and its radiative effect simulated by IPCC AR4 global models against ARM
surface observations. *Atmos. Chem. Phys.* 12, 1785–1810. doi:10.5194/acp-12-1785-2012,
2012.

Ramanathan, V., Cess, R.D., Harrison, E.F., Minnis, P., Barkstorm, B.R., Ahmad, E.,
Hartmann, D.: Cloud-Radiative Forcing and Climate: Results from the Earth Radiation
Budget Experiment. *Science* (80-.). 243, 57 LP-63,, 1989.

Randall, D.A.: Cloud parameterization for climate modeling: Status and prospects. *Atmos.*
Res. 23, 345–361. doi:[https://doi.org/10.1016/0169-8095\(89\)90025-2](https://doi.org/10.1016/0169-8095(89)90025-2), 1989.

Rao, T.N., Kirankumar, N.V.P., Radhakrishna, B., Rao, D.N., Nakamura, K.: Classification
of Tropical Precipitating Systems Using Wind Profiler Spectral Moments. Part II: Statistical
Characteristics of Rainfall Systems and Sensitivity Analysis. *J. Atmos. Ocean. Technol.* 25,
898–908. doi:10.1175/2007JTECHA1032.1, 2008a.

Ravi Kiran, V., Rajeevan, M., Gadhavi, H., Rao, S.V.B., Jayaraman, A.: Role of vertical
structure of cloud microphysical properties on cloud radiative forcing over the Asian

monsoon region. *Clim. Dyn.* 45, 3331–3345. doi:10.1007/s00382-015-2542-0, 2015.

Reddy, N.N., Rao, K.G.: Contrasting variations in the surface layer structure between the convective and non-convective periods in the summer monsoon season for Bangalore location during PRWONAM. *J. Atmos. Solar-Terrestrial Phys.* 167, 156-168. doi:10.1016/j.jastp.2017.11.017, 2017, 2018.

Rind, D., Rossow, W.B.: The Effects of Physical Processes on the Hadley Circulation. *J. Atmos. Sci.* 41, 479–507. doi:10.1175/1520-0469(1984)041<0479:TEOPPO>2.0.CO;2, 1984.

Roja Raman, M., Jagannadha Rao, V.V.M., Venkat Ratnam, M., Rajeevan, M., Rao, S.V.B., Narayana Rao, D., Prabhakara Rao, N.: Characteristics of the Tropical Easterly Jet: Long-term trends and their features during active and break monsoon phases. *J. Geophys. Res. Atmos.* 114, n/a-n/a. doi:10.1029/2009JD012065, 2009.

Rossow, W. B. and Schiffer, R. A.: ISCCP Cloud Data Products, *B. Am. Meteorol. Soc.*, 72, 2–20, doi:10.1175/1520-0477(1991)072<0002:ICDP>2.0.CO;2, 1991.

Rossow, W.B., Garder, L.C.: Validation of ISCCP Cloud Detections. *J. Clim.* 6, 2370–2393. doi:10.1175/1520-0442(1993)006<2370:VOICD>2.0.CO;2, 1993.

Rossow, W.B., Lacis, A.A.: Global, Seasonal Cloud Variations from Satellite Radiance Measurements. Part II. Cloud Properties and Radiative Effects. *J. Clim.* 3, 1204–1253. doi:10.1175/1520-0442(1990)003<1204:GSCVFS>2.0.CO;2, 1990.

Rossow, W.B., Zhang, Y.: Evaluation of a Statistical Model of Cloud Vertical Structure Using Combined CloudSat and CALIPSO Cloud Layer Profiles. *J. Clim.* 23, 6641–6653. doi:10.1175/2010JCLI3734.1, 2010.

Rossow, W.B., Zhang, Y., Wang, J.: A Statistical Model of Cloud Vertical Structure Based on Reconciling Cloud Layer Amounts Inferred from Satellites and Radiosonde Humidity Profiles. *J. Clim.* 18, 3587–3605. doi:10.1175/JCLI3479.1, 2005.

795 Sassen, K., Wang, Z.: Classifying clouds around the globe with the CloudSat radar: 1-year of
796 results. *Geophys. Res. Lett.* 35, n/a-n/a. doi:10.1029/2007GL032591, 2008.

797 Seiz, G., Tjemkes, S., and Watts, P.: Multiview Cloud-Top Height and Wind Retrieval with
798 Photogrammetric Methods: Application to Meteosat-8 HRV Observations, *J. Appl. Meteorol.*
799 *Clim.*, 46,1182–1195, doi:10.1175/JAM2532.1, 2007.

800 Slingo, A., Slingo, J.M.: The response of a general circulation model to cloud longwave
801 radiative forcing. I: Introduction and initial experiments. *Q. J. R. Meteorol. Soc.* 114, 1027–
802 1062. doi:10.1002/qj.49711448209, 1988.

803 Slingo, J.M., Slingo, A.: The response of a general circulation model to cloud longwave
804 radiative forcing. II: Further studies. *Q. J. R. Meteorol. Soc.* 117, 333–364.
805 doi:10.1002/qj.49711749805, 1991.

806 Stephens, G.L.: Cloud Feedbacks in the Climate System: A Critical Review. *J. Clim.* 18,
807 237–273. doi:10.1175/JCLI-3243.1, 2005.

808 Stephens, G.L., Vane, D.G., Tanelli, S., Im, E., Durden, S., Rokey, M., Reinke, D., Partain,
809 P., Mace, G.G., Austin, R., L’Ecuyer, T., Haynes, J., Lebsock, M., Suzuki, K., Waliser, D.,
810 Wu, D., Kay, J., Gettelman, A., Wang, Z., Marchand, R.: CloudSat mission: Performance and
811 early science after the first year of operation. *J. Geophys. Res. Atmos.* 113, n/a-n/a.
812 doi:10.1029/2008JD009982, 2008.

813 Subrahmanyam, K.V., Kumar, K.K.: CloudSat observations of multi layered clouds across
814 the globe. *Clim. Dyn.* 49, 327–341. doi:10.1007/s00382-016-3345-7, 2017.

815 Uma, K.N., Kumar, K.K., Shankar Das, S., Rao, T.N., Satyanarayana, T.M.: On the Vertical
816 Distribution of Mean Vertical Velocities in the Convective Regions during the Wet and Dry
817 Spells of the Monsoon over Gadanki. *Mon. Weather Rev.* 140, 398–410. doi:10.1175/MWR-
818 D-11-00044.1, 2012.

819 Venkat Ratnam, M., Narendra Babu, A., Jagannadha Rao, V.V.M., Vijaya Bhaskar Rao, S.,

820 Narayana Rao, D.: MST radar and radiosonde observations of inertia-gravity wave
821 climatology over tropical stations: Source mechanisms. *J. Geophys. Res. Atmos.* 113, n/a-n/a.
822 doi:10.1029/2007JD008986, 2008.

823 Venkat Ratnam, M., Pravalika, N., Ravindra Babu, S., Basha, G., Pramitha, M., Krishna
824 Murthy, B. V.: Assessment of GPS radiosonde descent data. *Atmos. Meas. Tech.* 7, 1011–
825 1025. doi:10.5194/amt-7-1011-2014, 2014a.

826 Venkat Ratnam, M., Sunilkumar, S. V, Parameswaran, K., Krishna Murthy, B. V,
827 Ramkumar, G., Rajeev, K., Basha, G., Ravindra Babu, S., Muhsin, M., Kumar Mishra, M.,
828 Hemanth Kumar, A., Akhil Raj, S.T., Pramitha, M.: Tropical tropopause dynamics (TTD)
829 campaigns over Indian region: An overview. *J. Atmos. Solar-Terrestrial Phys.* 121, 229–239.
830 doi:<https://doi.org/10.1016/j.jastp.2014.05.007>, 2014b.

831 Wang, F., Xin, X., Wang, Z., Cheng, Y., Zhang, J., Yang, S.: Evaluation of cloud vertical
832 structure simulated by recent BCC_AGCM versions through comparison with CALIPSO-
833 GOCCP data. *Adv. Atmos. Sci.* 31, 721–733. doi:10.1007/s00376-013-3099-7, 2014.

834 Wang, J., Rossow, W.B.: Effects of Cloud Vertical Structure on Atmospheric Circulation in
835 the GISS GCM. *J. Clim.* 11, 3010–3029. doi:10.1175/1520-
836 0442(1998)011<3010:EOCVSO>2.0.CO;2, 1998.

837 Wang, J., Rossow, W.B.: Determination of Cloud Vertical Structure from Upper-Air
838 Observations. *J. Appl. Meteorol.* 34, 2243–2258. doi:10.1175/1520-
839 0450(1995)034<2243:DOCVSF>2.0.CO;2, 1995.

840 Wang, J., Rossow, W.B., Uttal, T., Rozendaal, M.: Variability of Cloud Vertical Structure
841 during ASTEX Observed from a Combination of Rawinsonde, Radar, Ceilometer, and
842 Satellite. *Mon. Weather Rev.* 127, 2484–2502. doi:10.1175/1520-
843 0493(1999)127<2484:VOCVSD>2.0.CO;2, 1999.

844 Wang, J., Rossow, W.B., Zhang, Y.: Cloud Vertical Structure and Its Variations from a 20-Yr

845 Global Rawinsonde Dataset. J. Clim. 13, 3041–3056. doi:10.1175/1520-
846 0442(2000)013<3041:CVSAIV>2.0.CO;2, 2000.

847 Warren, S.G., Hahn, C.J., London, J., Chervin, R.M., Jenne, R.L.: Global distribution of total
848 cloud cover and cloud type amounts over the ocean. doi:TN-317+STR, 212 pp, 1988.

849 Wielicki, B.A., Harrison, E.F., Cess, R.D., King, M.D., Randall, D.A. Mission to Planet
850 Earth: Role of Clouds and Radiation in Climate. Bull. Am. Meteorol. Soc. 76, 2125–2153.
851 doi:10.1175/1520-0477(1995)076<2125:MTPERO>2.0.CO;2, 1995.

852 Winker, D.M., Hunt, W.H., McGill, M.J.; Initial performance assessment of CALIOP.
853 Geophys. Res. Lett. 34, n/a-n/a. doi:10.1029/2007GL030135, 2007.

854 Wu, D. L., Ackerman, S. a., Davies, R., Diner, D. J., Garay, M. J., Kahn, B. H., Maddux, B.
855 C., Moroney, C. M., Stephens, G. L., Veefkind, J. P., and Vaughan, M. A.: Vertical
856 distributions and relationships of cloud occurrence frequency as observed by MISR, AIRS,
857 MODIS, OMI, CALIPSO, and CloudSat, Geophys. Res. Lett., 36, L09821,
858 doi:10.1029/2009GL037464, 2009.

859 Xi, B., Dong, X., Minnis, P., Khaiyer, M.M.: A 10 year climatology of cloud fraction and
860 vertical distribution derived from both surface and GOES observations over the DOE ARM
861 SPG site. J. Geophys. Res. Atmos. 115, n/a-n/a. doi:10.1029/2009JD012800, 2010.

862 Yang, Q., Fu, Q., Hu, Y.: Radiative impacts of clouds in the tropical tropopause layer. J.
863 Geophys. Res. Atmos. 115, n/a-n/a. doi:10.1029/2009JD012393, 2010.

864 Zhang, J., Chen, H., Li, Z., Fan, X., Peng, L., Yu, Y., Cribb, M.: Analysis of cloud layer
865 structure in Shouxian, China using RS92 radiosonde aided by 95 GHz cloud radar. J.
866 Geophys. Res. Atmos. 115, n/a-n/a. doi:10.1029/2010JD014030, 2010.

867 Zuidema, P.: Convective Clouds over the Bay of Bengal. Mon. Weather Rev. 131, 780–798.
868 doi:10.1175/1520-0493(2003)131<0780:CCOTBO>2.0.CO;2, 2003.

Tables:

	Height-resolving RH thresholds		
Altitude range	min-RH	max-RH	inter-RH
0-2 km	92%	95%	84%
2-6 km	90%	93%	82%
6-12 km	88%	90%	78%
>12 km	75%	80%	70%

Table 1. Summary of height-resolving RH thresholds.

	Multi-layer clouds	Cloud base altitude (km)	Cloud top altitude (km)	Cloud thickness (km)
	Single-layer cloud	6.32	9.24	2.92
Upper layer	two-layer clouds	8.51	11.23	2.72
	three-layer clouds	9.63	11.79	2.16
Middle layer	three-layer clouds	6.69	7.80	1.11
Lower layer	two-layer clouds	4.08	5.56	1.48
	three-layer clouds	3.04	4.31	1.27

Table 2. Mean base, top and thicknesses of cloud layers of single-layer, two-layer and three-layer clouds.

Figures:

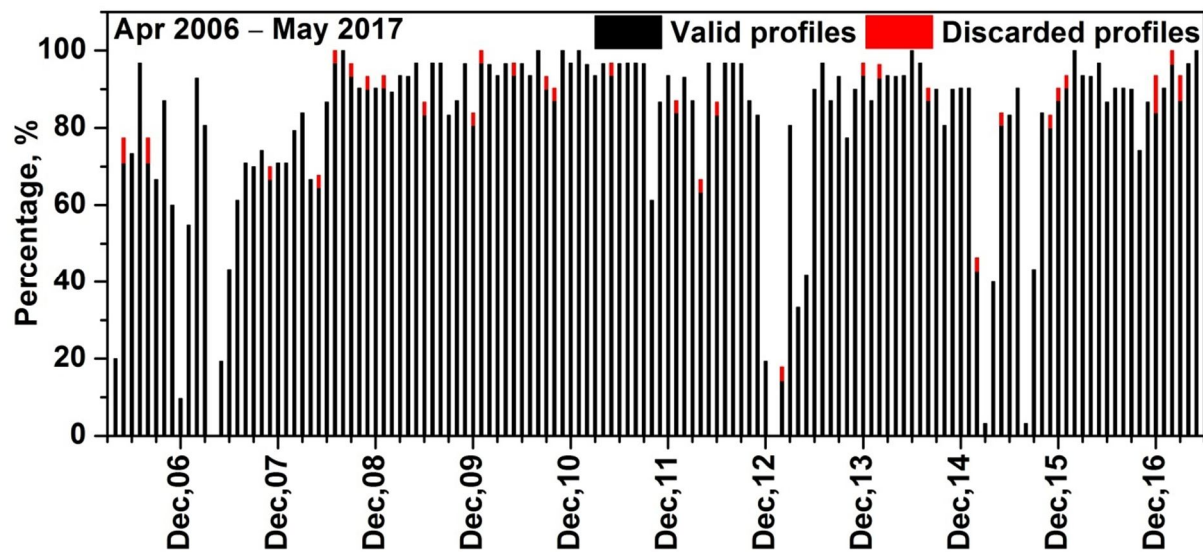


Figure 1. Monthly percentage of radiosonde data available during Apr. 2006 – May 2017 at Gadanki. Percentage of discarded profiles in each month is also shown with red colour.

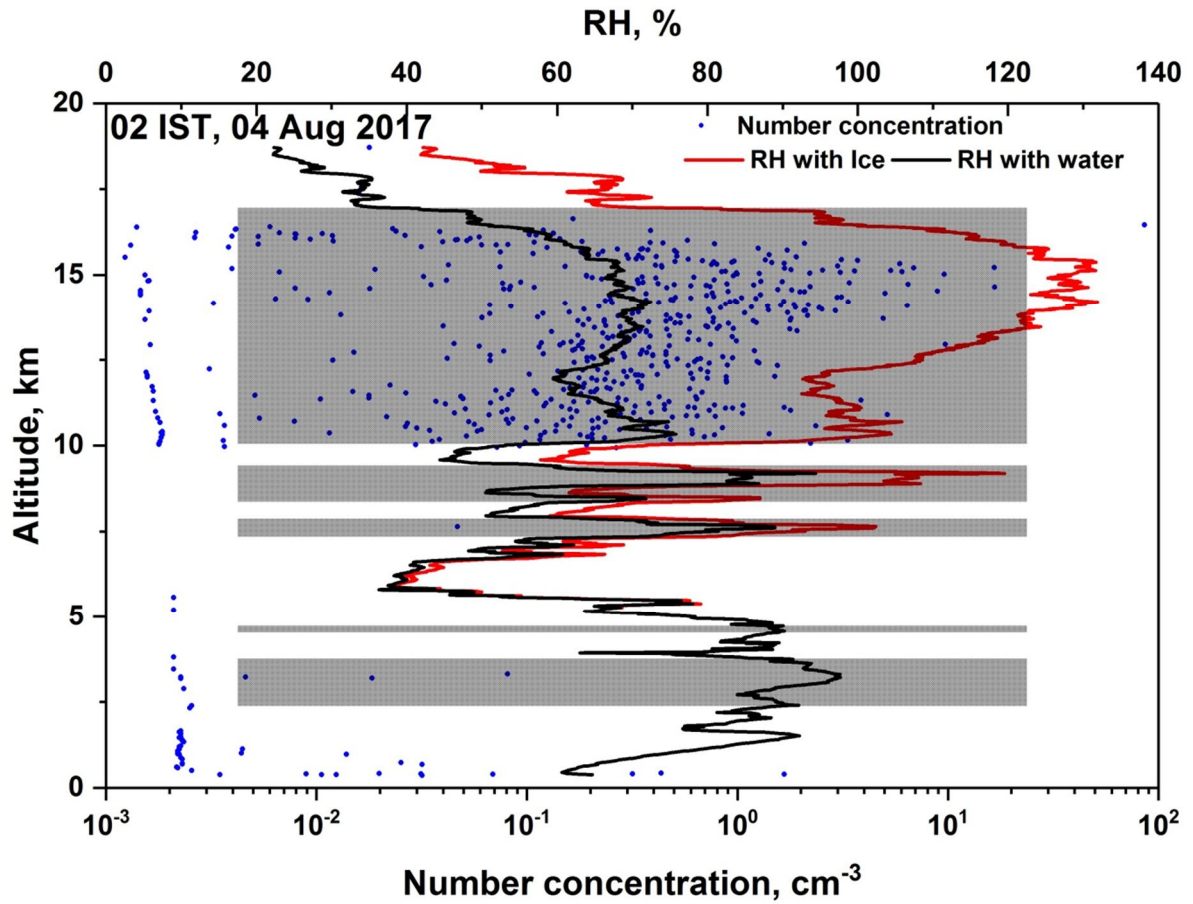


Figure 2. Results from a flight of RS-11G radiosonde and Cloud Particle Sensor (CPS) sonde on the same balloon launched at 02 IST on 04 Aug, 2017 at Gadanki, India. Profiles of RH estimated with respect to water (black solid line) and ice (when temperatures are less than 0°C (red solid line)), and number concentration (filled blue circles) from CPS sonde profile are shown. Detected cloud layer boundaries are shown by the filled gray rectangle boxes. Increase in the number concentration within the detected cloud layers indicates the cloud layer boundaries detected in the present study are accurate.

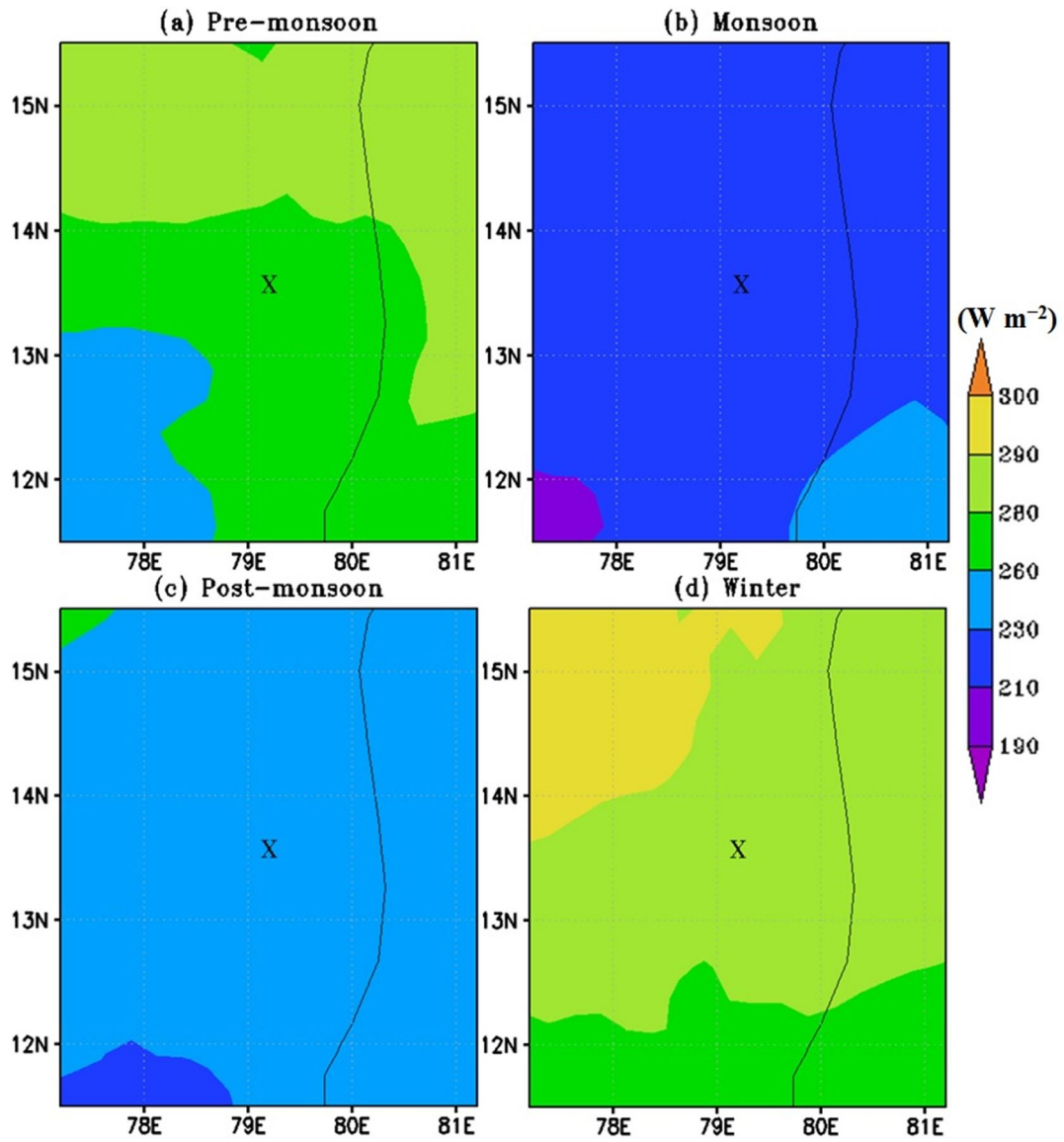


Figure 3. Seasonal mean distribution of OLR around Gadanki location observed during (a) Pre-monsoon, (b) Monsoon, (c) Post-monsoon and (d) Winter seasons averaged during 2006 – 2017. The symbol ‘X’ indicates the location of Gadanki.

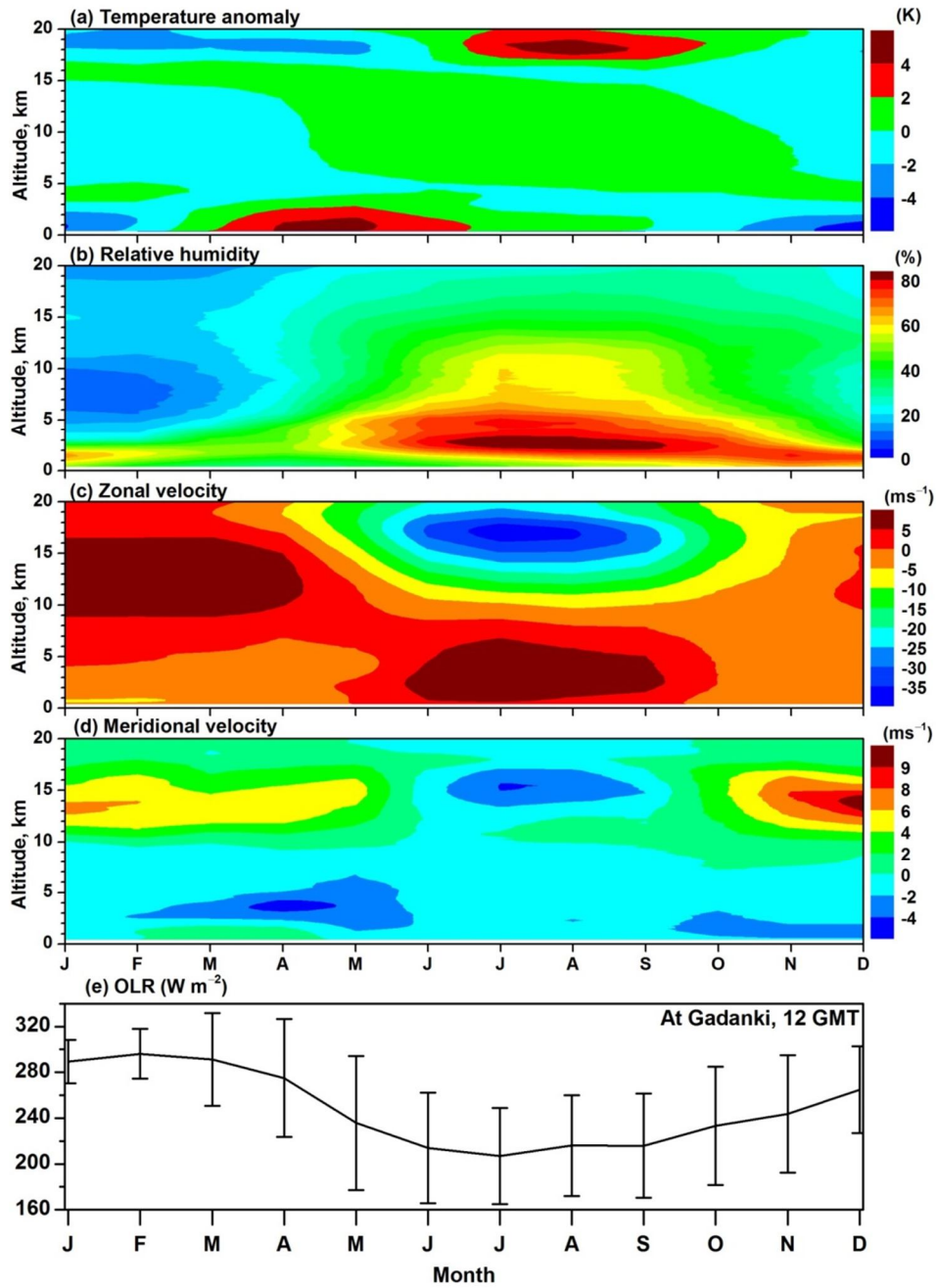


Figure 4. Time–altitude cross sections of monthly mean (a) Temperature anomaly, (b) Relative humidity, (c) Zonal wind and (d) Meridional wind observed over Gadanki using radiosonde observations during Apr. 2006 to May 2017. (e) Monthly mean Outgoing Longwave Radiation (OLR) over Gadanki obtained using KALPANA-1 data during Apr. 2006 to May 2017 along with standard deviation (vertical bars).

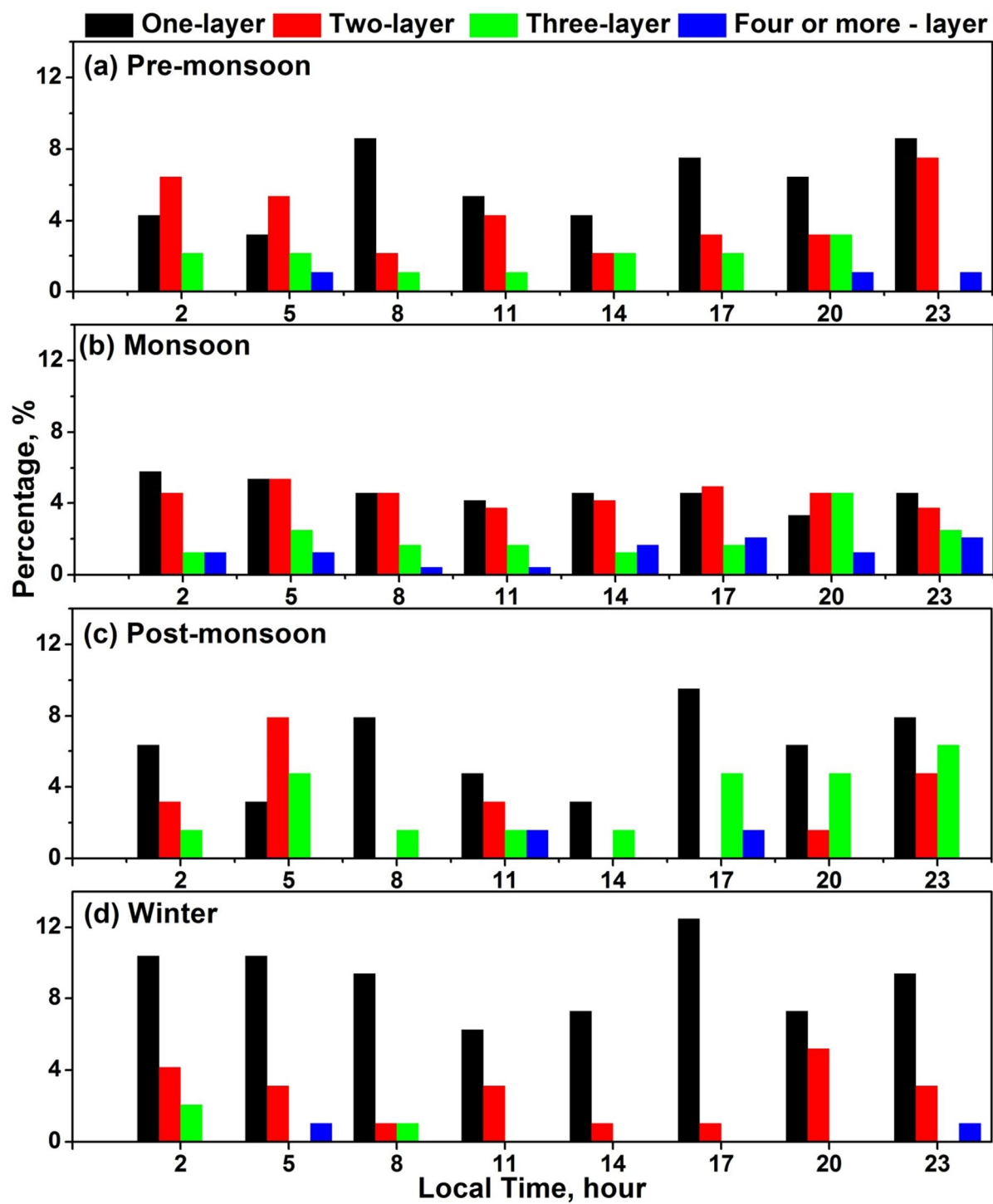


Figure 5. Diurnal variations of one-layer, two-layer, three-layer, and four- or more- layer clouds observed during (a) pre-monsoon, (b) monsoon, (c) post-monsoon, and (d) winter seasons.

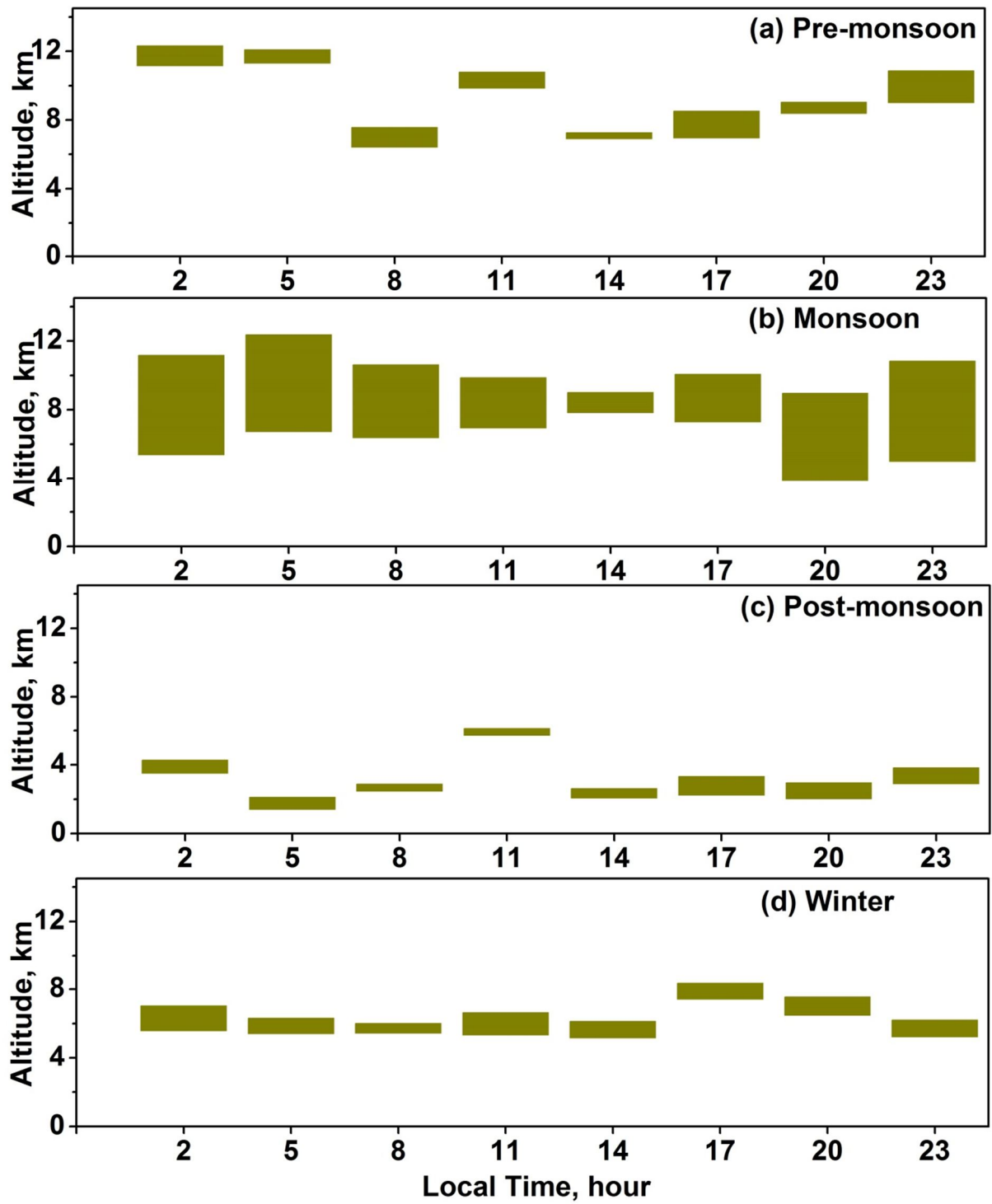


Figure 6. Diurnal variations of mean vertical locations (base and top), thicknesses of one-layer clouds observed during (a) pre-monsoon, (b) monsoon, (c) post-monsoon, and (d) winter seasons.

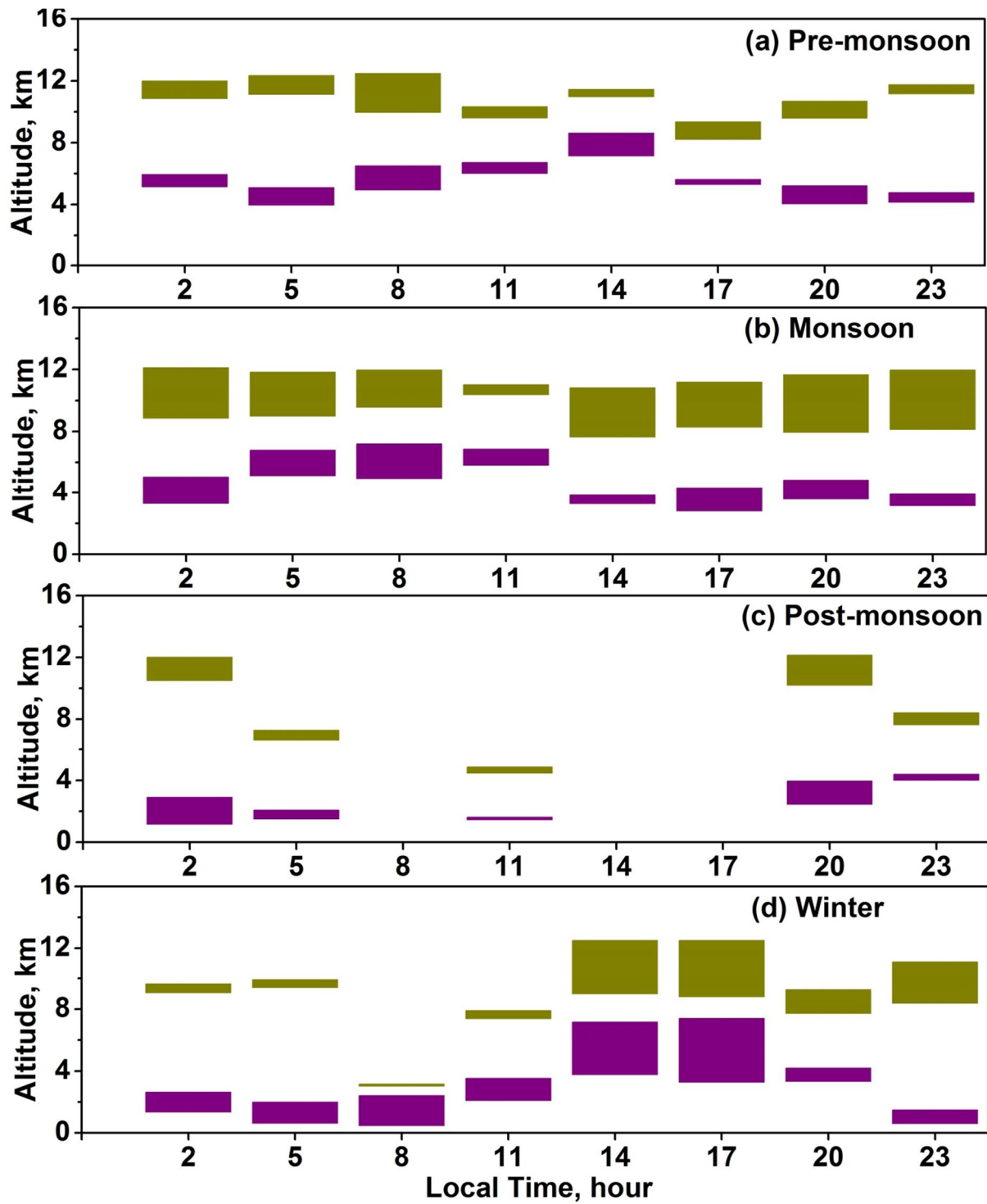
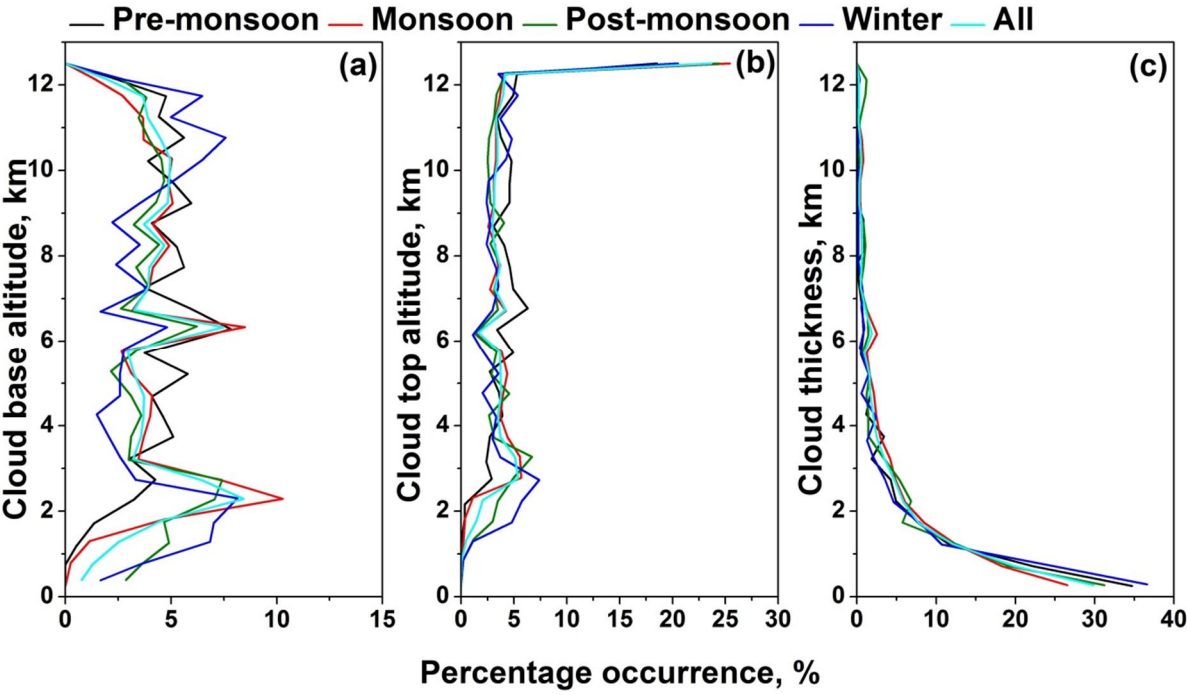


Figure 7. Diurnal variations of mean vertical locations (base and top), thicknesses of two-layer clouds observed during (a) pre-monsoon, (b) monsoon, (c) post-monsoon, and (d) winter seasons.



927

928 **Figure 8.** Percentage occurrence of the (a) cloud base altitude, (b) cloud top altitude and (c)
929 cloud thickness observed during different seasons over Gadanki. Altitude bin size is 500 m.

930

931

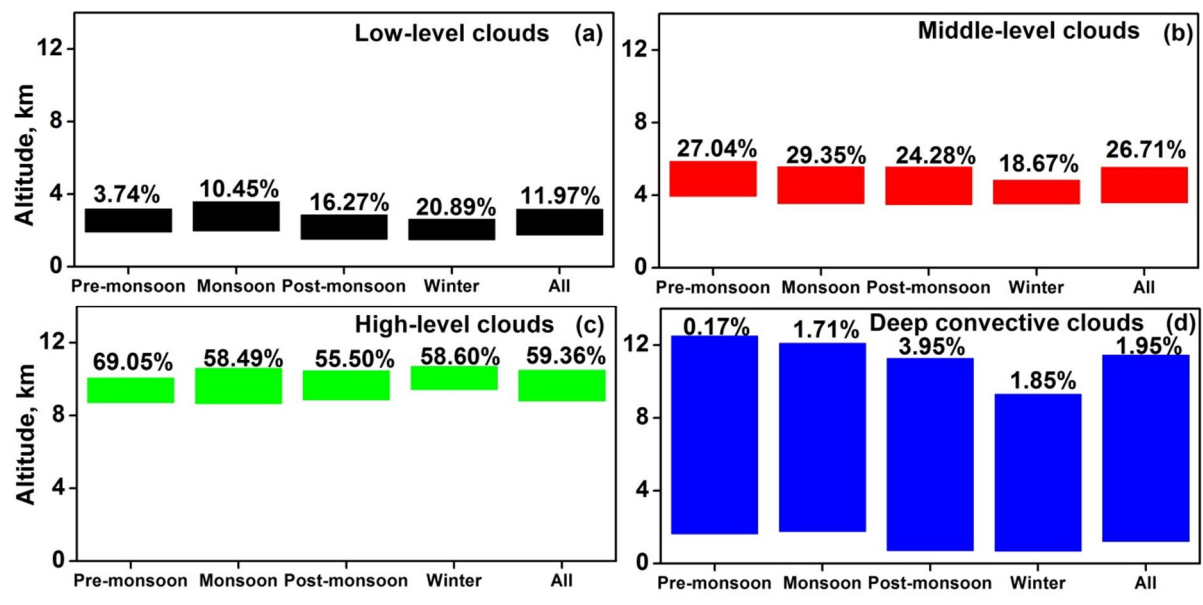


Figure 9. Mean vertical locations (base and top), cloud thicknesses and percentage occurrence of (a) low-level clouds, (b) middle-level clouds, (c) high-level clouds and (d) Deep convective clouds observed during different seasons.

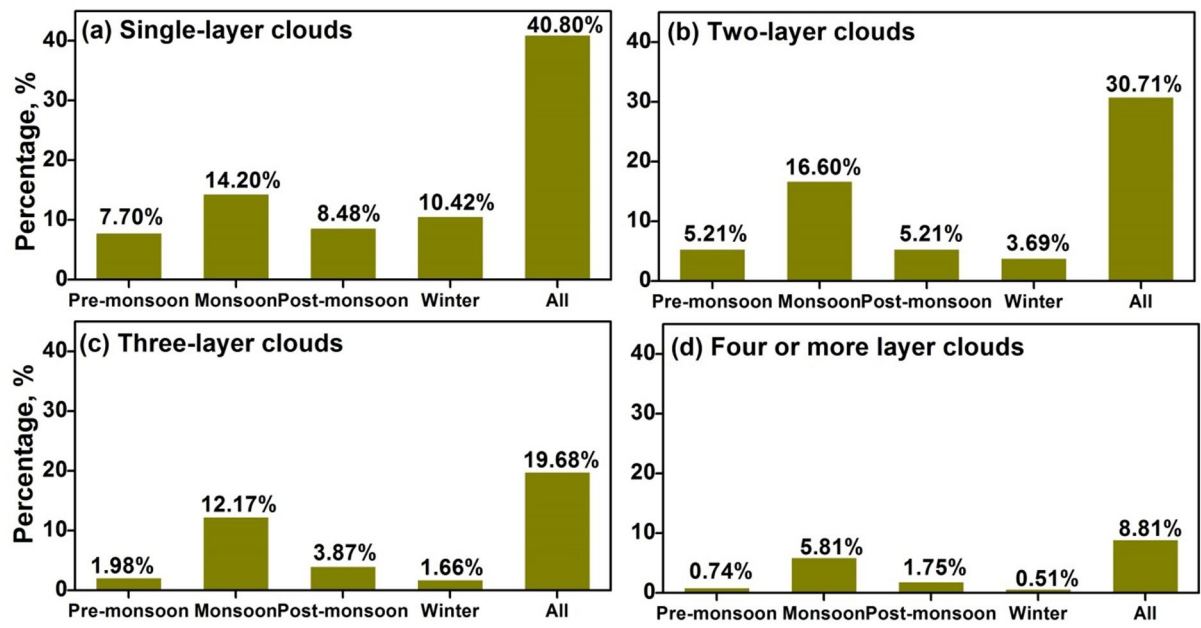


Figure 10. Percentage occurrence of (a) one-layer, (b) two-layer, (c) three-layer, and (d) four- or more- layer clouds observed during different seasons.

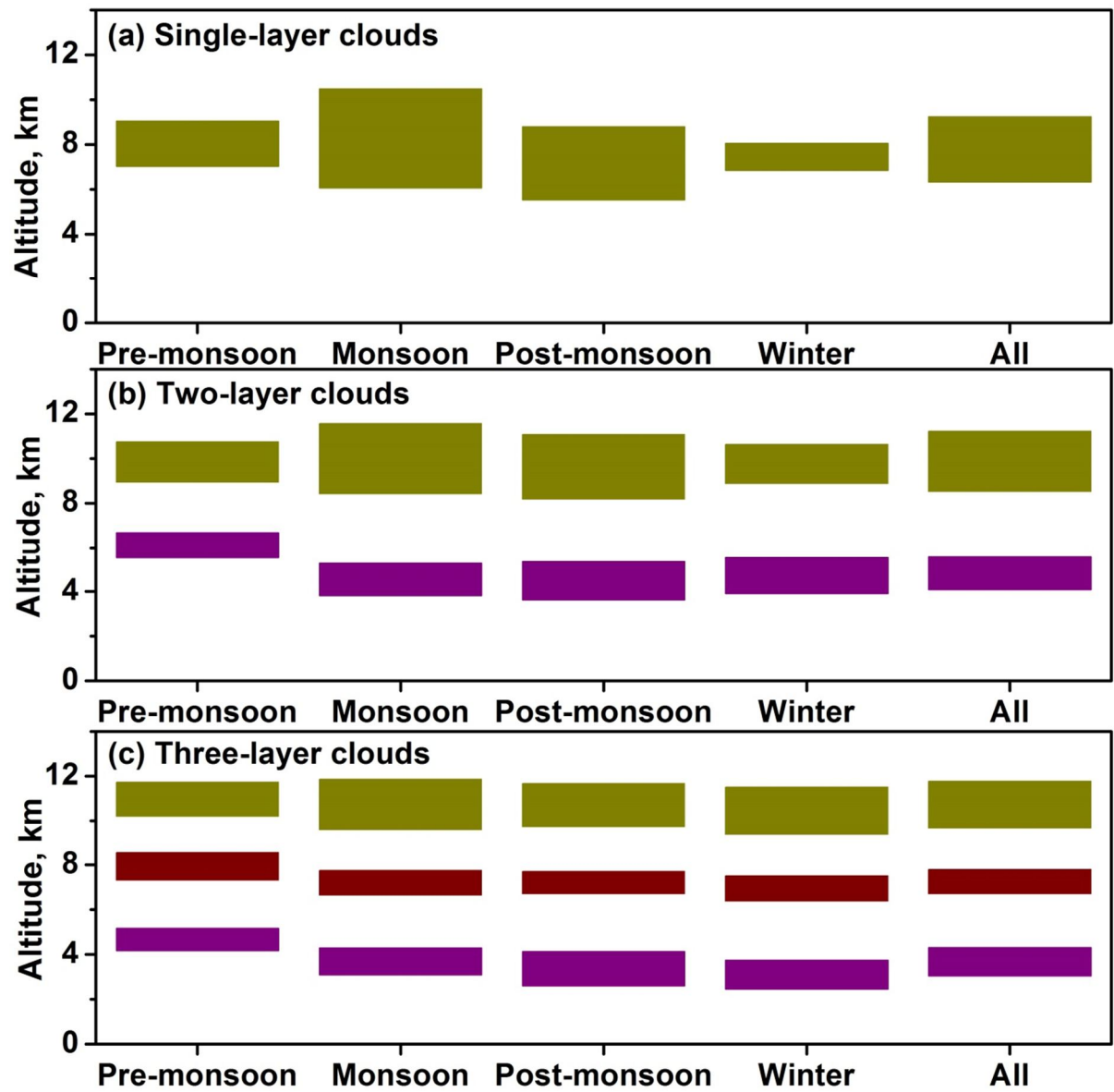


Figure 11. Mean vertical locations (base and top), cloud thicknesses of (a) one-layer clouds, (b) two-layer clouds, (c) three-layer clouds observed during different seasons.

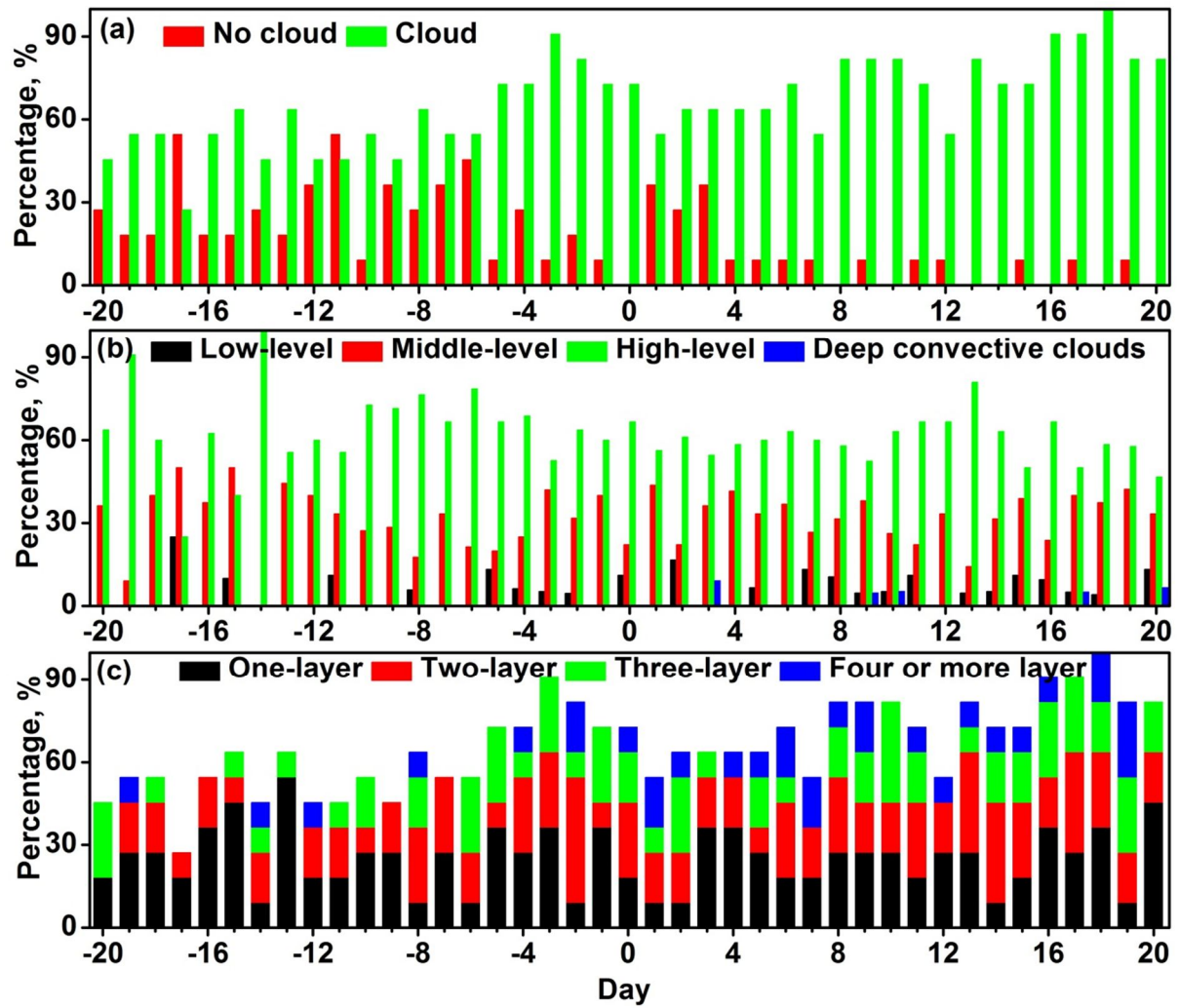


Figure 12. Composite (2006-2016) percentage occurrence of (a) clear and cloud conditions, (b) low-level, middle-level, high-level and deep convective cloud, and (c) one-, two-, three- and four or more- layer clouds observed with respect to the date of monsoon arrival over Gadanki location. Zero in x-axis indicates the date of monsoon arrival over Gadanki location.

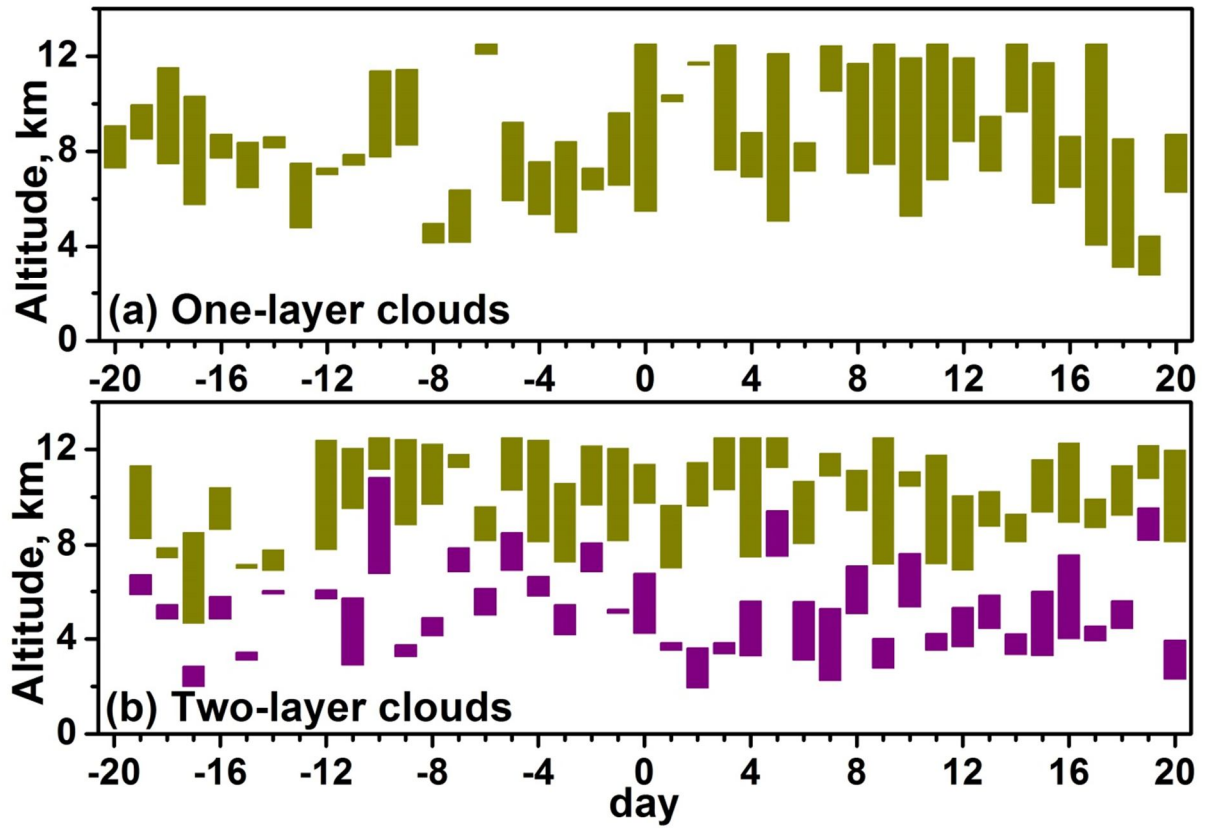


Figure 13. Composite (2006-2016) variations of mean vertical locations (base and top), thicknesses of one-layer clouds and two-layer clouds observed with respect to the date of monsoon arrival over Gadanki location. Zero in x-axis indicates the date of monsoon arrival over Gadanki location.

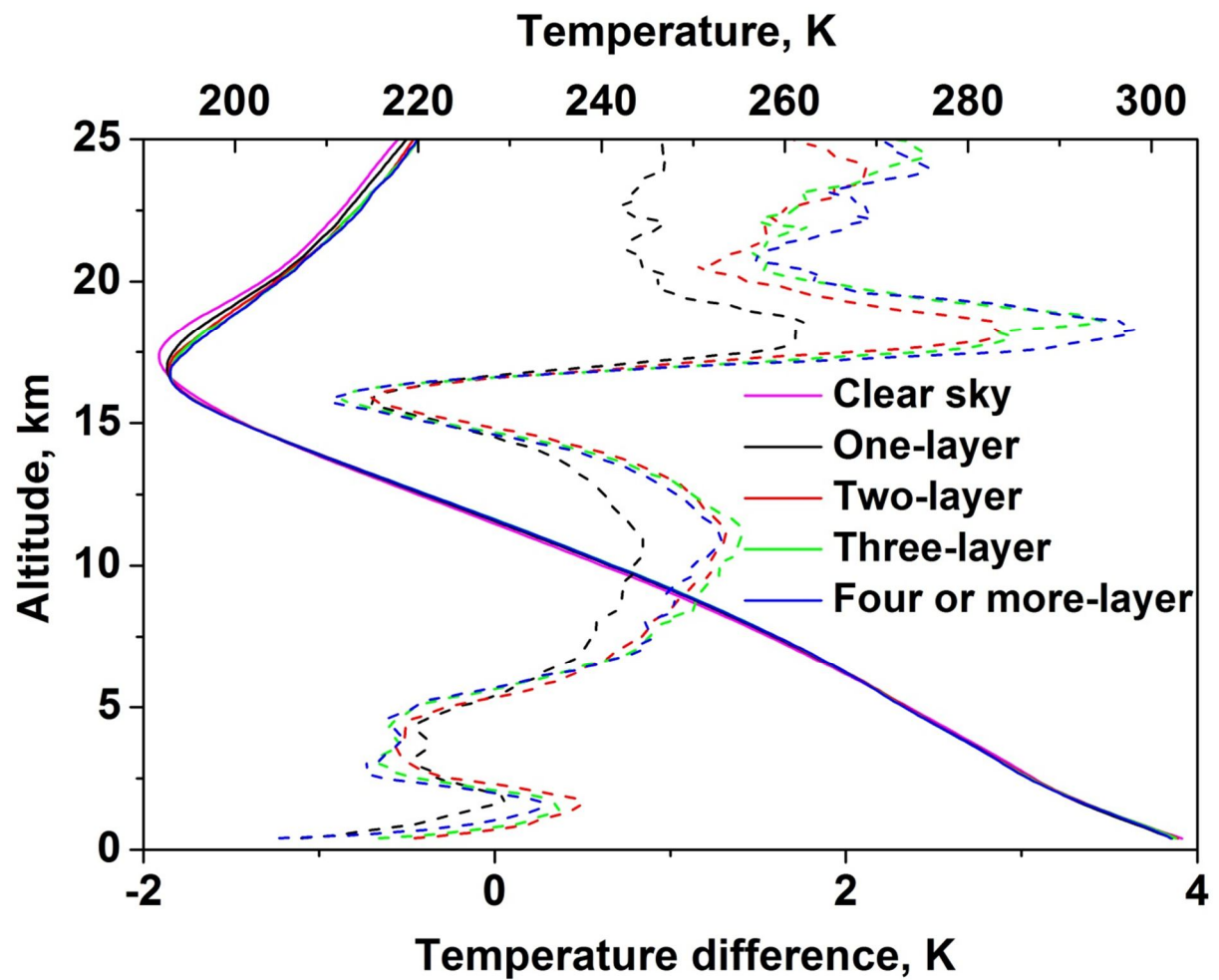


Figure 14. Composite (2006 – 2016) temperature profiles during clear sky, one-layer, two-layer, three-layer and four or more-layer cloud occurrences. The respective temperature difference profiles from clear sky conditions are shown with dash lines.